Screening of chemical libraries for new antifungal drugs against *Aspergillus fumigatus* reveals the potential mechanism of action of miltefosine

Thaila Fernanda dos Reis[1,2], Maria Augusta Crivelente Horta[1], Ana Cristina Colabardini[1], Caroline Mota Fernandes[3], Lilian Pereira Silva[1], Rafael Wesley Bastos[1], Maria Vitória de Lazari Fonseca[1], Fang Wang[4], Celso Martins[5], Márcio L. Rodrigues[6,7], Cristina Silva Pereira[5], Maurizio Del Poeta[3,8,9,10], Koon Ho Wong[4,11,12] and Gustavo H. Goldman[1]

[1]Faculdade de Ciências Farmacêuticas de Ribeirão Preto, Universidade de São Paulo, Ribeirão Preto, Brazil;
[2]MicroControl Innovation Ltda, Ribeirão Preto, São Paulo, Brazil
[3]Department of Microbiology and Immunology, Stony Brook University, Stony Brook, New York, USA;
[4]Faculty of Health Sciences, University of Macau, Macau SAR of China;
[5]Instituto de Tecnologia Química e Biológica António Xavier, Universidade Nova de Lisboa (ITQB NOVA), Oeiras, Portugal;
[6]Instituto Carlos Chagas (ICC), Fundação Oswaldo Cruz – Fiocruz, Curitiba/PR, Brazil;
[7]Instituto de Microbiologia Paulo de Góes, Universidade Federal do Rio de Janeiro (UFRJ), Rio de Janeiro/RJ, Brazil;
[8]Veteran Administration Medical Center, Northport, New York, USA;
[9]MicroRid Technologies Inc., 86 Deer Park Road, Dix Hills, New York, USA;
[10]Division of Infectious Diseases, School of Medicine, Stony Brook University, New York, USA
[11]Institute of Translational Medicine, Faculty of Health Sciences, University of Macau, Avenida da Universidade, Taipa, Macau SAR of China;
[12]MoE Frontiers Science Center for Precision Oncology, University of Macau.

Keywords: *Aspergillus fumigatus,* drug repurposing, miltefosine, sphingolipids, transcription factor

Corresponding author: Dr. Gustavo H. Goldman
Departamento de Ciências Farmacêuticas
Faculdade de Ciências Farmacêuticas de Ribeirão Preto, Universidade de São Paulo, Av. do Café S/N, CEP 14040-903, Ribeirão Preto, São Paulo, Brazil, Phone/Fax: 55-16-33154280/81, e-mail address: ggoldman@usp.br

69

70 ## Abstract

71

72 *Aspergillus fumigatus* is an important fungal pathogen and the main etiological
73 agent of aspergillosis, a disease characterized by a noninvasive process that can
74 evolve to a more severe clinical manifestation called invasive pulmonary
75 aspergillosis (IPA) in immunocompromised patients. The antifungal arsenal to
76 threat aspergillosis is very restricted. Azoles are the main therapeutic approach
77 to control IPA, but the emergence of azole-resistant *A. fumigatus* isolates has
78 significantly increased over the last decades. Therefore, new strategies are
79 necessary to combat aspergillosis and drug repurposing has emerged as an
80 efficient and alternative approach for identifying new antifungal drugs. Here, we
81 used a screening approach to analyze *A. fumigatus* in vitro susceptibility to 1,127
82 compounds. *A. fumigatus* was more susceptible to 10 compounds, including
83 miltefosine, a drug that displayed fungicidal activity against *A. fumigatus*. By
84 screening an *A. fumigatus* transcription factor null library, we identified a single
85 mutant, which has the *rmiA* (resistant to miltefosine) gene deleted, conferring a
86 phenotype of susceptibility to miltefosine. The transcriptional profiling (RNA-seq)
87 of the wild-type and the Δ*rmiA* strains and the Chromatin Immunoprecipitation
88 coupled to next generation sequencing (ChIP-Seq) of a RmiA-tagged strain
89 exposed to miltefosine revealed genes of the sphingolipids pathway that are
90 directly or indirectly regulated by RmiA. Sphingolipids analysis demonstrated that
91 the mutant has overall decreased levels of sphingolipids when growing in the
92 presence of miltefosine. The identification of RmiA represents the first genetic
93 element described and characterized which plays a direct role in miltefosine
94 response in fungi.

Author summary

The filamentous fungus *Aspergillus fumigatus* causes a group of diseases named aspergillosis and their development occurs after the inhalation of conidia dispersed in the environment. Very few classes of antifungal drugs are available for aspergillosis treatment, *e.g.*, azoles, but the emergence of global resistance to azoles in *A. fumigatus* clinical isolates has increased over the last decades. Repositioning or repurposing drugs already available on the market is an interesting and faster opportunity for the identification of novel antifungals agents. By using a repurposing strategy, we identified 10 different compounds that impact *A. fumigatus* survival. One of these compounds, miltefosine, demonstrated fungicidal activity against *A. fumigatus*. The mechanism of action of miltefosine is unknown and aiming to get more insights about it, we identified a transcription factor RmiA (Resistant to miltefosine) important for miltefosine resistance. Our results suggest that miltefosine plays antifungal activity against *A. fumigatus* interfering in the sphingolipids biosynthesis.

Introduction

Fungi are widespread in nature surviving as saprophytic organisms or associated with animals and plants where they can behave as commensal or opportunistic organisms. In humans, pathogenic fungi can cause both superficial and invasive infections giving rise to the death of millions of people annually (1–3). *Cryptococcus, Candida, Aspergillus*, and *Pneumocystis spp* are responsible for the most representative invasive fungal infections (1) showing death rates as high as tuberculosis and malaria (2, 4, 5). The levels of mortality are dependent on the host immune system integrity, being particularly important for immunocompromised patients (6–8). These individuals comprise a risk group that is expanding quickly due to the increasing number of immune-deficient patients who underwent transplant or chemotherapy, and patients under therapy with high dosage of corticosteroids (9–11).

Aspergillus spp. cause a group of diseases collectively named aspergillosis and their development occur after the inhalation of conidia dispersed in the environment (12). In immunocompetent patients the development of aspergillosis is mainly characterized by noninvasive diseases including aspergilloma, chronic necrotizing pulmonary aspergillosis, chronic cavitary pulmonary aspergillosis, and chronic fibrotic pulmonary aspergillosis, which are together defined as chronic pulmonary aspergillosis (12–16). These diseases present different manifestations but are in general related to a preexisting cavitary lung disease and classical features of systemic fungal disease are always absent (17, 18). Additionally, the allergic bronchopulmonary aspergillosis (ABPA) is a severe atopic disease caused by *Aspergillus*, mainly *A. fumigatus* (19, 20). The disease originates from the sensitization to fungal allergens of the host who present high levels of IgE (21). Patients with cystic fibrosis and other genetic diseases that affect the respiratory system are more predisposed to ABPA (19, 22, 23). Finally, the invasive pulmonary aspergillosis (IPA) is an important clinical manifestation caused by *Aspergillus* spp. presenting high levels of mortality in immunocompromised patients (1, 24). IPA is the most common invasive fungal infection in recipients of both hematopoietic stem cells and solid-organ transplants (1, 24). In this group of high-risk patients for IPA, *A. fumigatus*

147 represents the major cause of the disease reaching up to 90% of mortality (9–12,
148 25).

149 Very few classes of antifungal drugs are available for IPA treatment, such
150 as polyenes (amphotericin B), azoles (itraconazole, posaconazole, voriconazole,
151 and isavuconazole), and echinocandins (caspofungin) (26–29). Although both
152 amphotericin B and echinocandins can be used to treat IPA, these drugs have
153 clinical limitations. Amphotericin B shows high levels of nephrotoxicity and side
154 effects while echinocandins are not fully recommended as monotherapy for IPA
155 (9, 13, 30–32). So far, the administration of triazoles is the first therapeutic
156 approach applied to control *A. fumigatus* infections showing the most prominent
157 usage in the medical field (13, 33). Among them, itraconazole (introduced in
158 1990s), voriconazole (introduced in 2002) and posaconazole (introduced in 2006)
159 are the most common drugs utilized for the treatment of aspergillosis (34).
160 Voriconazole is the primary treatment against IPA followed by liposomal
161 amphotericin B (L-AMB) and echinocandins, which are recommended as a
162 second line therapy (35) (13, 33). Moreover, the activity of isavuconazole, a new
163 extended-spectrum triazole drug, has been recently tested against *Aspergillus*
164 (36–39).

165 The number of azole-resistant *A. fumigatus* clinical isolates has
166 dramatically increased over the last decades has become a major concern (35,
167 40–45). Additionally, azoles are also used in the agriculture to combat plant
168 pathogenic fungi and recently, its usage for agricultural purposes has been linked
169 to the emergence of azole-resistant isolates among human fungal pathogens (40,
170 46–49). Therefore, the emergence of global resistance to currently available
171 antifungals agents represent a significant threat to immunosuppressed patients,
172 as the current arsenal of antifungal drugs is very limited.

173 *A. fumigatus* has developed different azole resistance mechanisms, e.g.
174 amplification of the gene encoding the drug target, Cyp51/Erg11 14-alpha
175 demethylase; drug target modification, and/or overexpression of efflux pumps
176 (50–54). Specifically, These events are linked to amino acid substitution(s) in the
177 target Cyp51A protein, tandem repeat sequence insertions at the cyp51A
178 promoter, and overexpression of the ABC transporter Cdr1B (55–57). The
179 scenario became even more dramatic since the emergence of fungal isolates
180 intrinsically resistant to other commercial antifungals available. For instance,

Some clinical isolates of *A. flavus* and *A. terreus*, also responsible for cases of IPA, have been reported as intrinsically resistant to amphotericin B (12, 29, 58–61).

This situation highlights the need to understand the mechanisms of drug resistance and tolerance, and the search for novel antifungal agents (62, 63). As a few antifungal compounds are coming to market because their development is time-consuming and expensive, repositioning or repurposing drugs which are already licensed is an interesting and faster opportunity for the identification of novel antifungals agents (64–66). By using the repurposing strategy, many compounds have already been identified as new potential drugs against several diseases including parasitosis, protozooses and mycoses (64, 66–71). Here, screened two compound collection to analyze *A. fumigatus in vitro* susceptibility for compounds present in two compound libraries. The first library has active compounds against neglected diseases (The Pathogen Box) while the second one includes drugs previously approved for usage against human diseases [National Institutes of Health (NIH) clinical collection (NCC)]. We showed here that *A. fumigatus* was susceptible to at least 10 different compounds from the two libraries. One of these compounds, miltefosine, a drug mainly used in the treatment of visceral and cutaneous leishmaniasis (72, 73), demonstrated fungicidal activity against *A. fumigatus*. Aiming to get more insights about the mechanism of action of miltefosine, we screened an *A. fumigatus* transcription factor null mutant library (484 null mutants) and identified a single mutant highly sensitive to miltefosine. The gene deleted in this mutant was named *rmiA* (resistant to miltefosine). A combination of RNA seq transcriptome and Chromatin Immunoprecipitation (ChIP) coupled to next generation sequencing (Seq) studies revealed differentially expressed genes directly or indirectly regulated by RmiA. The sphingolipids profiling of the wild-type and the Δ*rmiA* strains exposed to miltefosine revealed that the mutant has overall lower levels of sphingolipids comparing to the wild-type. Our results suggest that miltefosine plays antifungal activity against *A. fumigatus* by directly interfering in the sphingolipids biosynthetic pathway.

Results

Screening of the Pathogen Box and NIH Clinical Library. In order to find known compounds that are active against *A. fumigatus*, we tested its susceptibility to two chemical drug libraries, (i) the Pathogen Box (containing 400 compounds, see https://www.mmv.org/mmv-org) and the National Institutes of Health (NIH) clinical collection (NCC) (containing 727 compounds; see https://pubchem.ncbi.nlm.nih.gov/source/NIH%20Clinical%20Collection) through Minimal Inhibitory Concentration (MIC) assays. In total, combining both libraries 1,127 compounds were assessed by using MIC values up to 25 µM. *A. fumigatus* was susceptible to four known antifungal agents present in these collections (posaconazole, difenoconazole, bitertanol and amphotericin B; MIC values 5 µM, 5 µM, 5 µM and 10 µM, respectively). These results supported the reliability of the screening approach. *A. fumigatus* was also susceptible to other compounds with MIC values ranging from 1.56 to 25 µM (Table 1). In Table 1, we describe the compound name, the MIC detected in our screening, the current usage purpose (Description) and the mode of action (if known) for the 10 compounds (Table 1). These compounds include: (i) two azole salts, econazole and oxiconazole, expected to inhibit to some extent *A. fumigatus* growth, (ii) fluvastatin, a statin drug class used for hypercholesterolemia treatment, (iii) mesoridazine, a piperidine neuroleptic drug, (iv) cisapride, a parasympathomimetic drug acting as a serotonin 5-HT_4 agonist, (v) indinavir sulfate, a protease inhibitor used in anti-HIV cocktails, (vi) enalaprilat, an angiotensin-converting enzyme inhibitor, (vii) vincristine sulfate, an inhibitor of microtubule formation in the mitotic spindle, (viii) iodoquinol, an anti-amoebiasis agent with unknown mechanism of action and (ix) miltefosine, an anti-Leishmania compound with unknown mechanism of action (Table 1).

To determine if these compounds are fungicidal or fungistatic, the *A. fumigatus* conidial viability was tested after 48 h of exposure to each compound at its corresponding MIC (Figure 1A). Five compounds (fluvastatin, cisapride, indinavir sulphate, vincristine sulphate, and miltefosine) had 100 % fungicidal while six had fungistatic mechanism of action with 80 to 95 % of conidial killing at MIC concentration (Figure 1A).

These results suggest that some of these compounds are fungicidal and can act directly in specific *A. fumigatus* cell targets while others (like cisapride and enalaprilat) could be a lead compound in antifungal drug discovery.

Miltefosine displays antagonistic interaction with myriocin, a sphingosine biosynthesis inhibitor. We decided to investigate miltefosine in more detail because it is a fungicidal drug with an unknown mechanism of action. The combination between drugs is commonly used in clinical practice aiming to potentialize the antifungal effect of the drugs (74). Furthermore, the combination assay can help unraveling the mechanism of action of the drugs and how this may vary according to the concentration (75). To check if miltefosine has any interaction with other antifungal drugs, we combined this compound (ranging from 0.001 to 8.0 µg/ml, MIC value of 10 µM corresponds to 4 µg/ml) with different antifungal drugs (Figures 1B to 1E). Miltefosine was combined with posaconazole [0.03 - 2.0 µg/ml], voriconazole [0.0007 - 0.5 µg/ml], amphothericin B [0.06 - 4.0 µg/ml] and caspofungin [4.0 - 256.0 µg/ml]) (Figures 1B to 1E). Using the checkerboard microdilution method, the interaction between miltefosine and the other compounds was determined through the fractional inhibitory concentration index (FICI). The interaction between the drugs was classified as synergic (FICI ≤ 0.5), indifferent (0.5 < FICI ≤4.0) or antagonic (FICI > 4.0) (76). Under the assayed conditions, the FICI index varied from 1- 2.5 in the combination of voriconazole and miltefosine, 1- 0.6 between posaconazole and miltefosine, 0.6 – 1.2 between amphothericin B and miltefosine and 1.0 -1.1 between caspofungin and miltefosine. These data show that the addition of miltefosine did not affect the antifungal effects of the tested clinical antifungals against *A. fumigatus* indicating that there is no interaction between them.

There are evidences in the literature showing that miltefosine can affect the sphingolipid metabolism in trypanosomatids (77, 78). To check if miltefosine could display any interaction with drugs that affect the cellular lipids biosynthesis, we combined different concentrations of miltefosine [0.001 to 8.0 µg/ml] and myriocin [2.0 – 128 µg/ml] (Figure 1F), an inhibitor of serine palmitoyltransferase, the first step in sphingosine biosynthesis (79). At low concentrations of the drugs, indifferent interaction was observed. Interestingly, at high concentrations, myriocin impaired the antifungal effects of miltefosine against *A. fumigatus*

demonstrating an antagonistic effect between these compounds (Figure 1F). Considering that myriocin has only one single target identified, this result may suggest that exist a component of the sphingolipid pathway important to the antifungal effect of miltefosine.

RmiA is the major transcription factor that mediates miltefosine response in *A. fumigatus*. To assess if there are transcriptional programs modulating the tolerance response to miltefosine, a library of 484 *A. fumigatus* transcription factor (TF) null mutants (80) was screened for sensitivity to miltefosine [0.001 to 8.0 µg/ml]. A primary screening using 96-well plates identified six TF null mutants with different susceptibilities to miltefosine. To validate the differential susceptibility of these mutants to miltefosine, the 6 TF null mutants were grown in the absence or presence of different miltefosine concentrations, and their radial growth were measured (Figure 2). When compared to the wild-type strain, we observed discrete differences in five of these mutant strains (Figure 2). The Δ*mcnB* (AFUA_5G05600 that encodes a homologue of *A. nidulans* McnB, a multicopy supressor of *A. nidulans nimA1*, (81) showed about 20 % growth inhibition (Figures 2A and 2B) while Δ*pacC* (AFUA_3G11970 that encodes PacC, a protein important for pH regulation (82) showed about 50 % inhibition compared to the wild-type strain at 8 µg/ml (Figure 2A and 2B). The Δ*sslA* (AFUA_5G04333 that encodes a homologue of *Saccharomyces cerevisiae* Ssl1p, a subunit of the general transcription factor TFIIH) has about 50 % growth inhibition compared to the wild-type strain at 8 µg/ml (Figures 2A and 2B). The Δ*sebA* (AFUA_4G09080 encodes a TF important to cope with different kinds of stress (83) showed a 40 % inhibition to miltefosine 8 µg/ml while the wild-type is inhibited 60 % at this concentration (Figures 2A and 2B). The AFUA_5G03030 null mutant has 65 % growth inhibition compared to the wild-type strain at miltefosine 8 µg/ml (Figure 2). Notably, the AFUA_2G12070 mutant was unable to grow at 4 µg/ml miltefosine (Figures 2A, 2B, 3A and 3B). AFUA_2G12070 encodes a 492 amino acids novel fungal Zn_2-Cys_6 transcription factor (http://pfam.xfam.org/family/PF00172#Zn2/Cys6). We named this gene *rmiA* (*r*esistant to *mi*ltefosine). The Δ*rmiA* was complemented and the complementing strain Δ*rmiA:rmiA*$^+$ presented a reversible phenotype in terms of miltefosine sensitivity indicating that the miltefosine sensitivity phenotype of Δ*rmiA* is due to

316 the specific deletion of the *rmiA* gene (Figures 3A and 3B). The Δ*rmiA* mutant has
317 no differential susceptibility to different stressing conditions such as growth on
318 increasing concentrations of NaCl, Calcofluor white, sorbitol, $CaCl_2$ and
319 menadione (Supplementary Figure S1).
320 Aiming to localize the RmiA, we constructed a functional C-terminal
321 RmiA:GFP strain (Supplementary Figure S2) that showed no fluorescence in the
322 absence of miltefosine (Figures 3C and 3D). However, when the RmiA:GFP strain
323 was shifted 15 minutes to MM supplemented with 3 µg/ml of miltefosine,
324 RmiA:GFP can be detected in about 50 % of the nuclei (Figures 3C and 3D). In
325 addition, we also constructed a functional RmiA:3xHA strain (Supplementary
326 Figure S2). This strain was grown in VMM and further exposed to RPMI
327 supplemented (or not) to an inhibitory concentration of miltefosine (12.5 µg/ml)
328 for 4 and 8 min. A very faint band of 54.3 kDa corresponding to RmiA:3xHA was
329 observed in the control not exposed to miltefosine while increased intensity bands
330 were observed in 4 and 8 h exposure to miltefosine (Figure 3E).
331 These results indicate that the RmiA protein quickly translocates to the
332 nucleus and its expression is also increased upon miltefosine exposure.
333
334 **Miltefosine induces necrosis-like cell death and increases mitochondrial**
335 **fragmentation in *A. fumigatus.*** *A. fumigatus* form mitochondrial tubular and
336 highly dynamic networks that are fragmented in the presence of antifungal and
337 oxidative stressing agents such as hydrogen peroxide (84, 85). This increased
338 mitochondrial fragmentation has been associated as a marker for cell death (85).
339 Propidium Iodide (PI) is a fluorescent DNA-binding dye that freely
340 penetrates cell membranes of dead or dying cells, but is excluded from
341 viable cells. Late apoptosis and early necrosis is characterized by an increased
342 number of PI-positive cells. To evaluate the effects of miltefosine and PI on the
343 mitochondrial morphology and viability, germlings from the wild-type, Δ*rmiA* and
344 Δ*rmiA::rmiA*$^{+}$ strains were treated with 3 µg/ml of the drug for 0, 5 or 10 min and
345 green MitoTracker (a mitochondrial fluorescent probe) or PI were added and
346 further analyzed by fluorescent microscopy (Figure 4A). In the absence of
347 miltefosine an intact mitochondrial network was observed in all the three strains.
348 However, upon 5 minutes of miltefosine exposure, the *ΔrmiA* cells showed about
349 60% of mitochondrial fragmentation evidenced by the presence of a punctuated

fluorescent pattern observed in the cytoplasm of the cells (Figures 4A and 4B), while in the wild-type and complemented strains the levels of mitochondrial fragmentation were much lower, 20 and 30 %, respectively (Figures 4A and 4B). When the wild-type and the Δ*rmiA::rmiA*+ germlings were left unexposed to miltefosine, about 5% of cells were stained by PI while in the Δ*rmiA* strain this level was about 7% (Figure 4C). However, upon miltefosine addition, the wild-type and the Δ*rmiA::rmiA*$^{+}$ germlings were about 12% stained by PI (Figure 4C).,while more than 50% of the Δ*rmiA* germlings showed PI staining (Figure 4C). These results suggest that miltefosine induces both mitochondrial fragmentation and necrosis cell death in *A. fumigatus.*, which was accentuated in Δ*rmiA*, emphasizing the importance of RmiA for survival and viability of *A. fumigatus*.

A. fumigatus germlings were exposed to 4 µg/ml of a functional fluorescent analogue of miltefosine, MT-11C-BDP [11-(4,4-Difluoro-1,3,5,7-tetrametil-4-bora-3a,4a-diaza-s-indacen-2-il) n-undecilfosfatidilcolina] (86) for about 5 minutes (Figure 5). MT-11C-BDP localizes to tubular structures that resemble mitochondrial networks and that were also fragmented in a fraction of the germlings (Figures 5A and 5B). Colocalization with MitoTracker^{TM} Deep Red FM indicated that MT-11C-BDP analogue is mainly localized at the mitochondria.

Miltefosine induces the modulation of genes encoding proteins responsible for the metabolism of lipids, fatty acid and derivatives. Aiming to get insights about genes that are modulated under miltefosine exposure, we carried out a transcriptomic analysis (RNA-seq) comparing *A. fumigatus* wild-type strain exposed to miltefosine. In comparison to the wild-type grown in MM, when the cells were shifted to RPMI medium supplemented with 3 µg/ml of miltefosine for 30 minutes, a total of 1,248 genes were upregulated (log2FC >1.0; *P*<0.005) and 940 genes were downregulated (log2FC <-1.0; P<0.005). In both cases the false-discovery rate (FDR) was less than 0.05 (Supplementary Table S1).

The enrichment analysis using FunCat (https://elbe.hki-jena.de/fungifun/fungifun.php) showed a transcriptional upregulation of genes involved in vesicular and vacuolar transport, metabolism of glutamate, caspase activation, ABC transporters, osmosensing response, transport ATPases, stress response, proteasomal degradation, lipid transport and a high enrichment in lipid,

fatty acid, and isoprenoid metabolism (Figure 6A). Genes involved in nuclear transport, RNA transport, Mitochondrial transport, TCA cycle, nucleotide binding, unfolded protein response, aminoacyl-tRNA-synthetases, amino acid metabolism, rRNA processing, ribosome biogenesis and translation were downregulated upon miltefosine exposure (Figure 6A). These results suggest that under miltefosine treatment, *A. fumigatus* increases the expression of genes involved in fatty acid metabolism and transport, stress responses and specific transporters while represses mitochondrial functions (e.g. TCA cycle and mitochondrial transport) and amino acid and protein biosynthesis.

The *rmiA* is important for the induction of genes involved in lipid metabolism upon miltefosine exposure in *A. fumigatus*. To identify potential targets modulated by RmiA we performed the transcriptional profiling of the Δ*rmiA* null mutant under the same experimental design previously described for the wild-type strain. We identified 292 differentially expressed genes (DEGs), with 184 genes upregulated (log2FC >1.0; P<0.005) and 108 genes downregulated (log2FC <-1.0; P<0.005; FDR<0.05), upon miltefosine exposure (Supplementary Table S2). FunCat enrichment analysis has not shown categories for upregulated genes in the Δ*rmiA* mutant. However, FunCat for the downregulated genes in the Δ*rmiA* mutant exposed to miltefosine revealed enrichment for categories of genes encoding proteins involved in lipid, fatty acid and isoprenoid metabolism, NAD/NADP binding, homeostasis of protons, ribosomal proteins, electron transport and transport ATPases (Figure 6B).

A visual inspection of DEGs in both wild-type and Δ*rmiA* strains showed zinc finger proteins (AFUA_5G12760 and AFUA_6g02690), MFS transporters (AFUA_5G09780 and AFUA_7G01790) and a sensor histidine kinase regulator (AFUA_5G10020) with higher levels of expression in the Δ*rmiA* in comparison to the wild-type (Figure 6C). Genes involved in the metabolism of fatty acids (AFUA_4G00340, AFUA_2G12530, AFUA_6G07270, AFUA_5G10670, AFUA_8g02590), cytochrome P450 enzymes (AFUA_3g03930, AFUA_4G03800, AFUA_2G04290), cell division control protein (AFUA_2G17110), aldehyde dehydrogenase (AFUA_4G13500), isocitrate lyase (AFUA_4G13510) were downregulated in the Δ*rmiA* when compared to the wild-type strain (Figure 6C). Accordingly, the RNAseq data was validated by

417 performing real-time PCR on 3 selected genes that showed a very similar
418 expression pattern in comparison with data from the RNAseq (Figure 6D).
419 Taken together our data shows that in the wild-type strain, the lipid and
420 fatty acid metabolism are upregulated upon miltefosine exposure suggesting their
421 possible importance for survival in presence of this drug. On the other hand, the
422 deletion of *rmiA* gene leads to a deficiency in the lipid and fatty acid metabolism,
423 strongly suggesting that it could be linked to the higher sensitivity of this mutant
424 to miltefosine.
425
426 **RmiA binds to a discrete number of gene promoter regions specifically in**
427 **the presence of miltefosine.** Considering that RmiA seems to be a TF involved
428 in miltefosine resistance in *A. fumigatus*, we decided to identify potential direct
429 targets under RmiA control of this protein using the Chromatin
430 Immunoprecipitation coupled to DNA sequencing (ChIP-seq) approach. The
431 RmiA:3xHA strain (Supplementary Figure S2 and Figure 7A) was grown in MM
432 and further exposed to RPMI supplemented (or not) with miltefosine for 30 min.
433 After immune-precipitation using anti-HA antibody, samples were sequenced
434 using the Illumina HiSeq2500 platform, the reads were aligned to the A. *fumigatus*
435 Af293 reference strain and the program MACS2 was used for peak calling. The
436 peak intensity map showed that RmiA binding was enriched at the promoter
437 region of 12 specific genes which are present in different chromosomes: (i)
438 AFUA_2G08260 encoding a homologue of *S. cerevisiae* Oye2p, a NADPH
439 oxidoreductase containing flavin mononucleotide (FMN) that may be involved in
440 sterol metabolism, oxidative stress response, and programmed cell death
441 (www.yeastgenome.org), (ii) AFUA_3G03230 encoding a BZIP transcription
442 factor (www.fungidb.org), (iii) AFUA_3G07300 AtrA encoding an ABC multidrug
443 transporter (www.fungidb.org), (iv) AFUA_3G10770 encoding a homologue of *S.*
444 *cerevisiae* Rbs1p, a sphingoid long-chain base (LCB) efflux transporter; integral
445 membrane transporter that localizes to the plasma membrane and may transport
446 long chain bases (LCBs) from the cytoplasmic side toward the extracytoplasmic
447 side of the membrane; role in glycerophospholipid translocation
448 (www.yeastgenome.org), (v) AFUA_4G03800 encoding a cytochrome P450
449 alkane hydroxylase (www.fungidb.org), (vi) AFUA_4G13500 encoding a
450 homologue of *S. cerevisiae* Hfd1p, a dehydrogenase involved in ubiquinone and

sphingolipid metabolism, converting hexadecenal to hexadecenoic acid in sphingosine 1-phosphate catabolism, the human homologue of ALDH3A2, mutated in Sjogren-Larsson syndrome (www.yeasgenome.org and (87), (vii) AFUA_5G10670 encoding a protein that has domain(s) with predicted iron ion binding, oxidoreductase activity and role in fatty acid biosynthetic process, oxidation-reduction process (www.fungidb.org), (viii) AFUA_2G14410 encoding an orthologue that has a role in xanthophyll metabolic process (www.fungidb.org), (ix) AFUA_4G11270 encoding an unknown function hypothetical protein (www.fungidb.org), (x) AFUA_4G11280 encoding an orthologue that has dolichyl-phosphate-mannose-glycolipid alpha-mannosyltransferase activity and role in GPI anchor biosynthetic process (www.fungidb.org), (xi) AFUA_5G10660 encoding a pentatricopeptide repeat protein (www.fungidb.org), and (xii) AFUA_6G03320 encoding a MFS transporter (www.fungidb.org) (Figure 7A and Supplementary Table S3). The RmiA binding to these promoter regions happens specifically in presence of miltefosine suggesting that RmiA is important for the activity of those genes in the presence of this drug. Accordingly, the RNAseq data demonstrate that the expression levels of AFUA_2G08260, AFUA_3G03230, AFUA_3G07300, AFUA_3G10770, AFUA_4G03800, AFUA_4G13500, and AFUA_5G10670 are repressed in the Δ*rmiA* strain in comparison with the wild-type when both strains are exposed to miltefosine (Figure 7B and Supplementary Table S3).

To identify putative RmiA-binding motifs in *A. fumigatus,* we carried out Multiple Expectation maximum for Motif Elicitation (MEME) of the 500 nucleotides surrounding each peak sequence identified in the ChIP-seq. The results show the enrichment of two consensus DNA binding sequences for RmiA in the presence of miltefosine (Figure 7C). Two binding mofifs were predicted: 5´-CGGAG(G or C)AA-3´ (e-value of 5e-02) and 5´-AACNGAATGA-3´ (e-value of 3.8e-02).

Together, our data highlight the importance of RmiA for events involved with the miltefosine resistance process in *A. fumigatus* and suggest that genes potentially modulated by the RmiA binding have specific binding motifs for this protein. Several promoter regions of genes that are bound by RmiA encode proteins involved in lipid metabolism.

RmiA is important for sphingolipids biosynthesis. Our previous results suggest that myriocin, a sphingolipid (SL) inhibitor, impairs the antifungal activity of miltefosine (Figure 1F). Considering that the metabolism of lipids seems to be involved with miltefosine resistance and the TF RmiA is linked to this process, we performed the SLs profiling of both wild-type and Δ*rmiA* strains exposed to miltefosine. Both strains were grown in VMM for 16h and shifted to RPMI media supplemented (or not) with 3 μg/ml of miltefosine for 4h. The main SL intermediates starting from the branching point of the pathway (DHS; dihydrosphingosine) were then measured through mass spectrometry analysis and the results were expressed in fold increase or decrease compared to the control not exposed to miltefosine (Figure 8A).

The deletion of *rmiA* leads to an overall reduction of the analysed SLs when compared to the SL levels in the wild-type strain under the same conditions (Figure 8A). Interestingly, the reduction in SL levels occurs in both, acidic and neutral branches of the pathway, suggesting the deletion of *rmiA* affects the early steps of the SL biosynthetic process. The branching point of the SL pathway is DHS, the precursor of dihydroceramide (DHC; the first intermediary of the neutral branch) and the phytosphingosine (PHS; the first intermediary of the acidic branch). However, the DHS is also converted to dihydrosphingosine 1-phosphate (DHS-1P) starting the metabolic pathway where the DHS-1P is converted to glycerolipid through many enzymatic reactions (Figure 8A). Upon miltefosine exposure, there is an increase of DHS and a decrease in DHS-1P in the wild-type strain while the opposite is observed in the Δ*rmiA* mutant (Figure 8A). Phytosphingosine (PHS), ceramide (CER), hydroxyceramide (OH-CER), phosphoceramide (P-CER), hydroxyphosphoceramide (OH-PCER), glucoceramide (GLC-CER), and inositolphosphoryl-ceramide (IPC) are increased when the wild-type strain is exposed to miltefosine (Figure 8A). In contrast, all these sphingolipids were reduced in the Δ*rmiA* when exposed to miltefosine (Figure 8A). We investigated in our RNA seq dataset the expression levels of the genes that encode enzymes involved in the different steps of the SLs pathway (Figure 8B). We observed 5 genes (Lcb2, AFUA_1G11890; LagA, AFUA_6G10460; Sur2, AFUA_1G16850; and LagA, AFUA_6G10460) with reduced and 2 genes (AurA, AFUA_3G09960 and MitA, AFUA_6G04680) with increased expression when the wild-type was exposed to miltefosine (Figure 8B).

Interestingly, only one gene (Hfd1, AFUA_4G13500) is differentially expressed with reduced expression when the Δ*rmiA* mutant is exposed to miltefosine (Figure 8B). Taken together, our results suggest that miltefosine antifungal activity against *A. fumigatus* interferes directly in the SL biosynthesis pathway.

Azole-resistant clinical isolates of *A.* fumigatus are sensitive to miltefosine. to verify if miltefosine is a good candidate for therapy against azole resistant strains, we tested if miltefosine could inhibit *A. fumigatus* growth of 19 clinical isolates (in addition to CEA17 strain) with different levels of azole resistance by determining their MICs. We tested 9 azole-sensitive *A. fumigatus* strains (CEA17, CYP15-109, IF1S-F4, IFM59056, ISFT-021, IFM61407, MO68507, MO54056, and IFM59056) and also 10 azole-resistant isolates, with different resistance mechanisms, cultured from different sample sites from patients from Portugal, Japan, Belgium and Switzerland (88) (Table 2). The most common azole-resistance mechanisms include amino acid substitutions in the target Cyp51A protein and tandem repeat sequence insertions at the *cyp51A* promoter (54) The *cyp51A* gene is not mutated in the azole-resistant strains F16134, F14946, CYP15-117, CYP15-147, CYP15-75, CYP15-93, CYP15-106, and CYP15-115 (*cyp51A* was not sequenced in the CYP-15-91 strain), suggesting different mechanisms of azole resistance (88). In contrast, strains 1799392 and 20089320 have TR34 tandem repeats at the *cyp51A* promoter region and L98H amino acid replacement at the Cyp51A (89). All the azole-sensitive or –resistant clinical isolates have a MIC of 4 µg/ml of miltefosine (Table 2). These results strongly indicate that miltefosine can inhibit the growth of clinical isolates that have developed resistance to azoles through different mechanisms.

Miltefosine increases the survival of *Galleria mellonella* larvae infected with *A. fumigatus.* On the basis of its essential role in sphingolipid biosynthesis, we asked whether RmiA is important for *A. fumigatus* virulence. *G. mellonella* larvae ($n = 10$ for each strain) were infected with the wild-type, *rmiA* deletion and complementation strains, and survival was assessed over a time period of 10 days (Figure 9A). The wild-type, Δ*rmiA*, and Δ*rmiA::rmiA*$^{+}$ strains caused 90 to 100 % mortality after 9 to 10 days postinfection (p.i.) ($P < 0.001$, Figure 9A).

These results indicate that RmiA is not a key regulator of *A. fumigatus* pathogenesis in the *G. mellonella* model.

As a proof-of-principle of the *in vivo* antifungal activity of miltefosine, we tested its ability to control or reduce the *A. fumigatus* infection in *G. mellonella* larvae (Figures 9B and 9C). First, we tested three different concentrations of miltefosine (40, 60 and 80 mg/kg of the larva) aiming to verify the drug concentration that could cause minimal damage to the larvae. These miltefosine concentrations caused about 40 % mortality after 10 days ($P < 0.001$, Figure 9B). *A. fumigatus* infection of *G. mellonella* larvae combined with the different miltefosine concentrations resulted in about 50 % survival of the invertebrate host ($P < 0.001$, Figure 9C). These results indicate that miltefosine is able to control 50 % of the mortality caused by *A. fumigatus* infection in *G. mellonella*.

Discussion

In the last years, the incidence of fungal infections has grown dramatically leading to an increasing number of deaths worldwide (1, 2). The mortality rate is linked to a set of conditions such as the host immune system integrity, availability of an effective antifungal drug, and the occurrence of clinical resistant isolates (6, 7, 11, 28, 90). The invasive pulmonary aspergillosis (IPA) is a disease caused by the opportunistic human pathogen *A. fumigatus* and displays high levels of morbidity and mortality mainly in immunocompromised patients (1, 24). Azoles are the main drug used to control IPA but the azole-resistant *A. fumigatus* isolates have increased significantly over the last decade (35, 40–45).

Given this scenario, there is an urgent need for new antifungal therapies applied to control IPA and other fungal diseases. The development of new antifungal drugs raises challenges such as the high costs and the time required for development and licensing of new compounds. To circumvent the slowness and cost of developing new drugs, the screening of chemical libraries and repurposing of drugs that are already commercialized for other purposes is a great opportunity to discover new antifungal compounds (62, 64, 67, 71, 91–93). Here we screened the growth of *A. fumigatus* in the presence of compounds present in two drug libraries and identified 10 compounds, among them five

584 compounds already known as inhibitors of fungal growth including two azole-
585 derivatives (econazole nitrate, and oxiconazole nitrate), fluvastatin, that inhibits
586 ergosterol biosynthesis, and iodoquinol and miltefosine, drugs with an unknown
587 mechanism of action. To our knowledge, the other five identified compounds
588 (mesoridazine, cisapride, indinavir sulfate, enalaprilat, and vincristine sulfate) are
589 novel as antifungal agents and have not been reported before. We investigated
590 a possible mechanism of action for miltefosine, a chemical belonging to the
591 alkylphosphocholine class. Miltefosine is mainly localized in the mitochondria and
592 it has a MIC value of 4 µg/ml under *in vitro* conditions and we demonstrated that
593 miltefosine is able to inhibit to the same extent *A. fumigatus* growth of several
594 clinical isolates, including highly azole-resistant strains. Miltefosine was a drug
595 initially used as an anti-neoplastic drug (94) and for treatment against
596 trypanosomatids (95), and it is the first drug approved for oral treatment of
597 leishmaniasis (77). However, the mechanism of action of miltefosine is not fully
598 understood and not necessarily the same in different organisms, and the specific
599 target of miltefosine has not been identified yet. Recent studies in
600 trypanosomatids have suggested that miltefosine acts by: (i) altering the correct
601 functionality of the sterol and sphingolipid metabolism (77, 78), (ii) inhibiting the
602 phosphatidylcholine synthesis (96), and the membrane remodeling due to the
603 phospholipase action, thus contributing to changing membrane physical
604 properties (97), (iii) inhibiting cytochrome *c* oxidase (98), (iv) activating the
605 plasma membrane Ca^{+2} channel opened by the sphingolipid sphingosine and (v)
606 destabilizing the intracellular Ca^{+2} homeostasis (78). On the other hand, the
607 resistance phenotype to miltefosine in trypanosomatids has been linked to genes
608 belonging to lipid metabolism (99).

609 Concerning to its antifungal behavior, miltefosine has demonstrated to be
610 effective against different fungal species (100–111), however, its mode of action
611 remains to be clarified. Recent studies have suggested that miltefosine triggers
612 its antifungal effects by destabilizing cell membranes and inducing apoptosis
613 (102, 105, 110, 112, 113). Accordingly, Spadari and colleagues (2018)
614 demonstrated that for *Cryptococcus spp.* miltefosine affects the plasma
615 membrane permeability due its interaction with ergosterol and/or phospholipids
616 increasing the production of ROS and DNA fragmentation which culminates with
617 the fungal death by apoptosis (105). In addition, in *C. krusei,* the mode of action

of miltefosine is also supposed to be related to the binding of the drug to ergosterol in the cell membrane leading to the cell apoptosis (110).

We observed that at the MIC concentration, miltefosine displayed a fungicidal effect against *A. fumigatus,* corroborating with previous results presented for several fungal species such as *Cryptococcus* spp, *Candida* spp, and molds (101–106, 108–110, 114). Our studies showed that miltefosine could decrease 50 % *A. fumigatus* mortality in *G. mellonella* larvae. We have then decided to check if miltefosine could present any interaction with other antifungal drugs. Azoles such as posaconazole and voriconazole that act by inhibiting the ergosterol biosynthesis (115), amphothericin B that sequesters ergosterol from the cell membrane (116) and caspofungin that targets the glucan synthase Fks1 and inhibits the synthesis of β-(1,3) glucan (117) were included in our analysis and none of them showed interaction with miltefosine. Our results corroborated what was previously observed in *Aspergillus spp* where the interaction between these compounds with miltefosine was indifferent for 32 from 33 isolates (103). In contrast to our results, miltefosine has been reported to have synergy with posaconazole against *Fusarium oxysporum* and the mucormycetes (118). In addition, a recent study with *C. auris* demonstrated that for 25% of the isolates assessed there was a synergic activity between miltefosine and amphothericin B, with FICI=0.5 (110).

Sphingolipids (SL) are complex lipids composed of octadecacarbon alkaline blocks, synthesized from non-sphingolipid precursors, and representing one of the most abundant lipids in the eukaryotic cell membranes (119, 120). In fungi, SLs are involved in central cellular functions such as growth, pathogenesis, cell death, and signal transduction (121–123). The SL biosynthesis starts in the endoplasmic reticulum where the non-lipidic precursors serine and palmitoyl coenzyme A are condensed by the serine palmitoyltransferase enzyme (SPT) into 3-keto dihydrosphingosine. The SPT is specifically targeted by myriocin, a sphingolipid inhibitor (79). The interaction assay between miltefosine and myriocin showed that at high concentrations of both compounds, the FICI value was greater than 4.0 characterizing an antagonistic effect between these drugs (76). This implicates that sphingolipid metabolism may be important to the antifungal effect of miltefosine, corroborating with previous results obtained for other fungal species and trypanosomatids (77, 78, 105, 110).

We were able to identify a completely novel *A. fumigatus* transcription factor RmiA, linked to miltefosine resistance in this pathogen. This information came from a large-sale phenotypic screening of a collection of TF deletion mutants in presence of miltefosine. Although the deletion of six TFs somehow moderately impacted the growth of the mutant in presence of miltefosine, the Δ*rmiA* is the most sensitive mutant. RmiA is a novel and uncharacterized TF that codifies a putative Zn(II)Cys6 binuclear domain that translocates to the nucleus in presence of miltefosine and seems to be a key TF in the miltefosine response in *A. fumigatus*. Miltefosine at MIC completely abolished the Δ*rmiA* mutant growth and no additional phenotypes were observed under other stress conditions such as growth in presence of sub-inhibitory concentrations of posaconazole, voriconazole, caspofungin, NaCl, Calcofluor white, sorbitol, and $CaCl_2$. The Identification of the *rmiA* gene as a putative major TF involved in *A. fumigatus* response to miltefosine provided us with an opportunity to enquiry the molecular mechanisms that are regulated by this gene.

The transcriptional profiling through RNAseq assay with the wild-type strain in presence or absence of miltefosine indicated increased upregulation of genes involved in lipids/fatty acid transport and metabolism. In contrast, the RNAseq of the Δ*rmiA* mutant exposed to miltefosine shows exactly an opposite behavior. The lipid and fatty acid metabolism were the main category of down-regulated genes which strongly suggests that this TF participates directly or indirectly in the induction of genes involved in lipid metabolism, including genes involved in the biosynthesis of sphingolipids. The identification of RmiA represents the first genetic element described and characterized which plays a direct role in miltefosine response in fungi.

Our work provides opportunities for understanding the mechanism of action of miltefosine throughout the characterization of the genes that are differentially expressed in the Δ*rmiA* mutant. Further work will focus on the molecular characterization of these differentially expressed genes.

Materials and Methods

Media, strains and phenotypic characterization. The *Aspergillus spp.* used in this work are listed in the Table S1. Azole-resistant *Aspergillus fumigatus* strains were kindly provided by Katrien Lagrou and were isolated from different sources in Belgium, Switzerland, Portugal, EUA. All *Aspergillus* strains were grown in either solid minimal medium [MM: 1 % glucose (w/v), 50 mL of a 20× salt solution, trace elements, 2% agar (w/v) pH6.5] or solid complete medium [YAG: 2% glucose (w/v), 0.5% yeast extract(w/v), trace elements, 2% agar (w/v)] at 37°C. The composition of the trace elements and nitrate salts is described at Käfer, 1977. For RNAseq, ChIP-seq and lipidomics, conidia were germinated in RPMI-1640 media and transferred to liquid Vogel's Minimal Medium (VMM). For phenotypic characterization, plates containing solid MM were centrally inoculated with 10^5 spores of each strain in presence or absence of variable concentration of miltefosine [0-8µg/mL]. After 120h of incubation at 37°C, the radial growth was measured. All plates were grown in triplicate, and averages ± standard deviations (SD) of the data are plotted. All strains used in this work are listed in the Supplementary Table S4.

Library drug screenings. Two different drug libraries were screened for antifungal activity against *A. fumigatus* CEA17 strain: The Pathogen Box (https://www.mmv.org/mmv-open/pathogen-box) and the National Institutes of Health (NIH) clinical collection (NCC) (https://pubchem.ncbi.nlm.nih.gov/source/NIH%20Clinical%20Collection) . The Pathogen Box (https://www.mmv.org/) is a collection of 400 diverse, drug-like molecules with already described activity against different pathogens responsible for important neglected diseases such as malaria, tuberculosis, toxoplasmosis, and others. The NCC library is composed by a small molecule repository of 727 compounds which are part of screening library for the NIH Roadmap Molecular Libraries Screening Centers Network (MLSCN) corresponding to a collection of chemically diverse compounds that have been in phase I-III clinical trials (64).

For the primary screening, the drugs were diluted from 0.78-25µM in 200µL of MOPS [3-(N-morpholino) propanesulfonic acid] buffered RPMI 1640

(Life Technologies), pH 7, in 96-well plates. In each well a total of $1x10^4$ conidia of *A. fumigatus* wild-type strain was inoculated. Plates were incubated for 48h at 37°C without shaking. Wells containing only medium and DMSO were used as controls. Fungal growth inhibition was determined visually as a no-growth endpoint and those compounds were selected for further studies. All experiments were done in triplicate.

Fungicidal or fungistatic activity of the selected compounds was also assessed. Briefly, a total of $1x10^4$ conidia of *A. fumigatus* wild-type strain was inoculated in 96-wells plates, each well containing 200µL of MOPS buffered RMPI 1640 medium plus the lowest concentration of each compound that promoted the fungal growth inhibition in the primary screening. Plates were incubated 48h at 37°C without shaking. Following, 100 was plated in solid complete medium and incubated at 37°C for another 36h. Wells containing only medium and DMSO were used as controls. The number of viable colonies was determined by colony-forming unity (CFU) compared to the negative control (no drug), which had 100% survival. Results are expressed as means standard deviations (SD) of three independent experiments.

Minimal inhibitory concentration (MIC). The miltefosine drug used for minimal inhibitory concentration (MIC) assays was purchased from Sigma-Aldrich and solubilized in ethanol. The MIC was determined based on the M38-A2 protocol of the Clinical and Laboratory Standards Institute (125).

Briefly the assay was performed in 96-wells plates containing 200µL of MOPS buffered RPMI 1640 medium pH 7.0, supplemented with miltefosine [0-8µg/mL] and $1x10^4$ conidia of *A. fumigatus,* per well. Plates were incubated at 37°C without shaking for 48h. Wells containing only medium and ethanol were used as control. The MIC value was defined as the lowest concentration of miltefosine that visually inhibited 100% of fungal growth. All experiments were done in triplicate.

Assays for checking antifungal activity of drug combinations. We checked the interaction of miltefosine with several drugs including antifungals and lipid inhibitor using a checkerboard microdilution method. The drugs concentrations ranged from 0.001 to 8.0 µg/mL for miltefosine, 0.03 - 2.0 µg/mL for

posaconazole, 0.0007 - 0.5 µg/mL for voriconazole, 4.0 - 256.0 µg/mL for caspofungin and 0.06 - 4.0 µg/mL for amphotericin B and 2.0 – 128 µg/mL for myriocin. The plates were incubated at 37°C during 48h. The MIC endpoint was 100% of growth inhibition. The interaction was quantitatively evaluated by determining the fractional inhibitory concentration index (FICI): FICI = [MIC miltefosine in combination/MIC miltefosine] + [MIC clinical drug in combination/MIC clinical drug]. The FICI was calculated for all possible combinations of different concentrations (126). Also, interaction curves were constructed. The interaction between these drugs was classified as synergic if FICI ≤0.5, indifferent if 0.5 <FICI≤4.0, and antagonic for FICI >4.0 (76).

Construction of *A. fumigatus* mutants. To generate the RmiA:3xHA mutant, a 2.9Kb fragment encompassing the rmiA ORF and the 5´UTR region, along with the 1kb 3´UTR DNA sequence, were PCR amplified from CEA17 genomic DNA (gDNA) with primer pairs P1/P2 and P4/P5 respectively. The 0.8kb 3xHA-trpC fragment was amplified from the pOB430 plasmid with primers P10/P11, the prtA gene was amplified from the plasmid pPTRI with primers P8/P9.

The RmiA:GFP strain was constructed by the amplification of a 2.9Kb fragment encompassing the rmiA ORF and the 5´UTR region, along with the 1kb 3´UTR DNA sequence, were PCR amplified from CEA17 gDNA with primer pairs P1/P3 and P4/P5 respectively . The GFP-trpC fragment was amplified from the pOB435 plasmid with primers P10/P11, the prtA gene was amplified from the plasmid pPTRI with primers P8/P9.

The Δ*rmiA* strain was complemented generating the Δ*rmiA::rmiA*$^{+}$ lineage. Specifically, the fragment containing the 5´UTR plus the *rmiA* gene, along with the 1kb 3´UTR DNA sequence, were PCR amplified from CEA17 gDNA with primer pairs P1/P7 and P4/P5 respectively. In addition, these fragments were fused to the *ptrA* gene, which was previously PCR amplified from plasmid pPRTI (primers P8/P9).

All DNA cassettes (rmiA^{+}::prtA, rmiA::GFP::prtA, and rmiA::3xHA::prtA) were constructed by *in vivo* homologous recombination by using *S. cerevisiae* (127). Briefly, the set of fragments of each of the constructions along with the plasmid pRS426 digested with BamHI/EcoRI were transformed into the *S. cerevisiae* SC9721 strain. Whole cassettes rmiA^{+}::prtA, rmiA::GFP::prtA

and rmiA::3xHA::prtA were transformed into the *ΔrmiA* strain, candidates were selected by resistance to pyrithiamine and further verified via western blot, reversal of miltefosine sensitivity phenotype and/or protein functionality.

Primers used in this work are listed in the Supplementary Table S5. Additionally, the mutant strains constructed in the current work were performed into the background of the Δ*rmiA* strain. Positive candidates were selected in the presence of pyrithiamine, purified through three rounds of growth on plates, submitted to gDNA extraction, and confirmed by PCR.

Protein extraction and immunoblot analysis. A total of 1 x 10^6 conidia/mL of each strain was inoculated in 50 mL of Vogel's medium and grown at 37 °C for 16h under agitation. Mycelia were then washed with RPMI 1640 media and incubated in RPMI 1640 containing 12.5 μg/mL of miltefosine at 37°C for 0, 4 and 8h at 37°C with shaking. For protein extraction, mycelia were ground into liquid nitrogen and resuspended in 0.5mL of lysis buffer (10% (v/v) glycerol, 50 mM Tris-HCl pH 7.5, 1% (v/v) Triton X-100, 150 mM NaCl, 0.1% (w/v) SDS, 5 mM EDTA, 50 mM sodium fluoride, 5 mM sodium pyrophosphate, 50 mM -glycerophosphate, 5 mM sodium orthovanadate, 1 mM phenylmethylsulfonyl fluoride (PMSF), and 1x complete mini protease inhibitor (Roche Applied Science). Extracts were centrifuged at 16,000 g for 20 min at 4°C. The supernatants were collected, and the protein concentrations were determined using the Bradford assay (Bio-Rad). Then, 30μg of total protein extract from each sample were resolved in 10% (w/v) SDS-PAGE and transferred to a nitrocellulose membrane for a Western blot assay. Monoclonal anti-HA antibody (Sigma-aldrich) was used to confirm the RmiA::3xHA expression. In addition, anti-α-actin antibody was used to normalize the protein loading. The primary antibodies were detected using a horseradish peroxidase (HRP)-conjugated secondary antibody raised in mouse (Sigma-Aldrich). Chemiluminescent detection was achieved using an ECL Prime Western blotting detection kit (GE Healthcare). To detect these signals on blotted membranes, the ECL Prime Western blotting detection system (GE Healthcare, Little Chalfont, UK) and LAS1000 (Fujifilm, Tokyo, Japan) were used.

Real-time PCR analysis. Total cellular RNA was extracted using TRIzol reagent (Invitrogen, Life Technologies, Camarillo, CA, USA). Further, RNA was submitted to DNA digestion with RQ1 RNase-free DNase (Promega, Fitchburg, WI, USA) according to the manufacturer's instructions. The cDNA synthesis was performed by the ImProm-II™ Reverse Transcription System (Promega) and oligo(dT). The real-time OCR was performed using the ABI 7500 Fast Real-Time PCR System (Applied Biosystems, Foster City, CA, USA) and the SYBR Green PCR Master Mix kit (Applied Biosystems), according to manufacturer's instructions. Analysis were carried-out using three independent biological replicates. The mRNA quantity relative fold change data was calculated using standard curves (128) and normalized by the expression levels of the housekeeping β-tubulin gene. Primer sequences used in this study are listed in Supplementary Table S5.

RNA purification and preparation for RNA-Seq. A total of 10^6 spores/ml of *A. fumigatus* WT and Δ*rmiA* were inoculated in 50 ml of Vogel's medium and grown at 37 °C for 16h under agitation. The suspensions were centrifuged and washed with PBS. Mycelia was suspended in VMM media containing glucose supplemented with 3 μg/mL of miltefosine, or in the absence of any drug, and incubated at 37 °C for additional 30 min. Total RNA was extracted by Trizol method. Subsequently, 10 μg of total RNAs were subjected to RNA purification using DNase I (New England Biolabs Inc.) and the quality was checked on 2% agarose gel and verified using the Agilent Bioanalyser 2100 (Agilent technologies). RNAs selected for further analysis had a minimum RNA Integrity Number (RIN) value of 8.0. One μg of purified RNAs were used for library preparation using Illumina NEBNext® Ultra™ Directional RNA Library Prep Kit according to manufacturer's protocol and sequenced using the Illumina HiSeq2500 platform at the Genomics and Single Cells Analysis Core facility at the University of Macau. The expression levels were calculated in RPKM and for the differential expression analysis a log2FoldChange of $-1 \leq Log2FC \geq 1$ was applied to capture minimum 2 times perturbation on the expression levels, with the $P<0.005$ and false-discovery rate (FDR) lower than 0.05.

Chromatin preparation. A similar experimental design used for the RNA seq was used for the ChIP seq experiments. After growth, the cultures were added

with 1% formaldehyde for 20 minutes with gentle shaking at room temperature, then a final concentration of 0.5M glycine was added to further incubation for 10 minutes. The mycelia were collected by filtering and washed with cold water. The crosslinked mycelia were frozen in liquid nitrogen and frozen dried for 2 hours before lysis. The cell lysis was processed by 6 times beating for 3 minutes with ~100 µl volume of silica beads using Bullet Blender (Next Advance) with 3 minutes of cooling in between each cycle. Chromatins were extracted as described (129) and sonicated using the Qsonica Q800R at 100% amplitude with 10 seconds ON and 15 seconds OFF cycles for a total sonication time of 30 minutes. Chromatin concentration and size (100-500bp) were checked on 2% agarose gel, and the prepared chromatins were stored at -80 ℃ until use.

Chromatin Immuno-precipitation and sequencing library preparation. Immuno-precipitation was carried out using anti-HA antibody as described previously (130). Immuno-precipitated materials were purified using QIAGEN PCR clean-up kit, and multiplexed sequencing libraries were prepared as described (130) using NEBNext® Ultra™ II DNA Library Prep Kit for Illumina according to manufacturer's protocol. Libraries were checked and quantified using DNA High Sensitivity Bioanalyser assay, mixed in equal molar ratio and sequenced using the Illumina HiSeq2500 platform at the Genomics and Single Cells Analysis Core facility at the University of Macau.

Data mapping and bioinformatics analysis. Raw sequencing reads of ChIPseq experiments were quality-checked using FastQC (http://www.bioinformatics.babraham.ac.uk/projects/fastqc/) and aligned to Af293 reference genome (genome version s03-m05-r06) using Bowtie2 (version: 2.2.9) (131). For peaks calling, MACS2 was applied. In order to determine the presence of conserved RmiA DNA binding motifs we carried out a MEME (Multiple EM for Motif Elicitation)-ChIP analysis to search the 500 bp region surrounding the peaks identified in our ChIP-seq data (http://meme-suite.org).

Lipid analysis. A total of 10^6 spores/ml of *A. fumigatus* WT and ΔAfub_027770 were inoculated in 50 ml of Vogel's medium and grown at 37 °C for 16h under agitation. The suspensions were centrifuged and washed with PBS. Mycelia was

suspended in VMM media containing glucose supplemented with 3 μg/mL of miltefosine, or in the absence of any drug, and incubated at 37 °C for additional 4h. Prior to cell lysis, C17-sphingolipids were added to the samples (132, 133). Mandala extraction was carried out as described previously (134), with a few modifications. To facilitate the disruption of mycelia, the samples were vortexed and sonicated for 2 min in the presence of 0.2 g of glass beads. Then, the samples were submitted to Bligh and Dyer Extraction (135). A quarter of each sample obtained from the Bligh and Dyer Extraction was reserved for inorganic phosphate (Pi) determination, so the relative sphingolipid signal was normalized by the Pi abundance. The organic phase was transferred to a new tube and submitted to alkaline hydrolysis of phospholipids (136). Finally, the organic phase was dried and used for mass spectrometry analysis (133).

Statistical analysis. Grouped column plots with standard deviation error bars were used for representations of data. For comparisons with data from wild-type or control conditions, we performed one-tailed, paired *t* tests or one-way analysis of variance (ANOVA). All statistical analysis and graphics building were performed by using GraphPad Prism 5.00 (GraphPad Software).

Fluorescence microscopy. A total of 10^5 spores of each strain was inoculated on coverslips in 4 ml of MM medium for 16 h at 30°C. After, coverslips with adherent germlings were left untreated or miltefosine for different periods of time, as indicated. Staining procedures included: (i) 5 min of incubation in a solution with Propidium Iodide (PI [0.05mg/ml], Sigma Aldrich); (ii) 5min of incubation in a solution with MitoTracker Deep Red^{TM} FM dye ([250nM], Invitrogen); (iii) 10min of incubation in a solution containing Hoechst 33342 dye (20μg/mL, Molecular Probes, Eugene, OR, USA). Further, the coverslips were rinsed with phosphate-buffered saline (PBS; 140 mM NaCl, 2 mM KCl, 10 mM NaHPO4, 1.8 mM KH_2PO_4, pH 7.4). Slides were visualized on the Observer Z1 fluorescence microscope using a 100x objective oil immersion lens. Differential interference contrast images (DIC) and fluorescent images were captured with AxioCam camera (Carl Zeiss) and processed using AxioVision software (version 4.8). In each experiment, at least 50 gemlings were counted. For GFP the wavelength excitation was 450 to 490 nm and emission wavelength of 500 to 550 nm. For

MitoTracker Deep Red™ FM the wavelength abs/em was about 644/665 nm. For Hoechst [4,6-diamidino-2-phenylindole] staining, the excitation wavelength was 365 nm and emission wavelength 420-470 nm. For PI the wavelength excitation was 572/25 nm and emission wavelength was 629/62 nm.

Virulence analysis in *Galleria mellonella* model. The *Galleria mellonella* larvae were obtained by breeding adult larvae (137) weighting 275-330 mg. The larvae were kept in starvation in Petri dishes at 37° in the dark for 24 hours prior to infection. The larvae used for the experiment were in the sixth stage of development. For infection, fresh spores from each strain (mutants and wild-type) were used. The spores of each strain were counted using a hemocytometer. The stock concentration of spore suspensions used for infection was $2x10^8$ conidia/ml, and from this stock 5ul were used for larval infection ($1x10^6$ conidia/larva). The control group was composed of larvae inoculated with 5 µl of PBS to observe any possible death caused by physical trauma. The inoculum was performed using a Hamilton syringe (7000.5KH) and the conidia were inoculated into the lower left proleg of the larvae. After 30 minutes of the larvae being infected, treatment with miltefosine (M5571 Sigma-Aldrich) was carried out. The drug was rehydrated in distilled water as recommended by the manufacturer (102). The concentrations used for the treatments were 40, 60 and 80 mg/kg of the larvae and each larva was weighted individually, and the volume was adjusted to the pre-established concentrations. As a control for the treatments, we made three groups of larvae in which concentrations of 40, 60 and 80mg / kg were injected. The treatments were also injected into the lower right proleg of the larvae. After infection, the larvae were kept at 37 ° in Petri dishes in the dark and scored daily. Larvae were considered dead due to lack of movement in response to touch. The viability of the inoculum administered was determined by plating a serial dilution of the conidia in YAG medium. The statistical significance of the comparative survival values was calculated using the log rank analysis of Mantel-Cox and Gehan-Brestow-Wilcoxon by using the statistical analysis package Prism (138).

952 **Data availability statement.** The datasets generated for this study are available
953 on request to the corresponding author.
954

955 ## Funding information
956
957 This study was supported by the Brazilian funding agencies Fundação de Amparo
958 à Pesquisa do Estado de São Paulo (FAPESP, 2016/12948-7) and Conselho
959 Nacional de Desenvolvimento Científico e Tecnológico (CNPq). This work was
960 also supported by the National Institutes of Health grants AI136934 and AI125770
961 to MDP, and a Merit Grant I01BX002924 from the Veterans Affairs Program to
962 MDP. K.H.W. was supported by the Research Services and Knowledge Transfer
963 Office of the University of Macau (Grant number: MYRG2019-00099-FHS).
964

965 ## Conflict of Interest

966 The authors declare that the research was conducted in the absence of any
967 commercial or financial relationships that could be construed as a potential
968 conflict of interest. Dr. Maurizio Del Poeta, M.D. is a Co-Founder and Chief
969 Scientific Officer (CSO) of MicroRid Technologies Inc.; Dra Thaila Fernanda dos
970 Reis is a Co-Founder of MicroControl Innovation. MLR is currently on leave from
971 the position of associate professor at the Microbiology Institute of the Federal
972 University of Rio de Janeiro, Brazil.
973

974 ## References

975

976 1. Brown GD, Denning DW, Gow NAR, Levitz SM, Netea MG, White TC.
977 2012. Hidden killers: Human fungal infections. Sci Transl Med 4.

978 2. Brown GD, Denning DW, Levitz SM. 2012. Tackling human fungal
979 infections. Science (80-) 336:647.

980 3. Roemer T, Krysan DJ. 2014. Antifungal Drug Development: Challenges,
981 Unmet Clinical Needs, and New Approaches. Cold Spring Harb Perspect
982 Med 4:a019703.

983 4. Calderone R, Gay-Andrieu F, Li D, Sun N, Groutas W, Weerawarna P,
984 Prasad S, Alex D. 2014. Antifungal drug discovery: The process and

985 outcomes. Future Microbiol 9:791–805.

986 5. Denning DW, Bromley MJ. 2015. How to bolster the antifungal pipeline.
987 Science (80-) 347:1414–1416.

988 6. Mayer FL, Wilson D, Hube B. 2013. Candida albicans pathogenicity
989 mechanisms. Virulence 4:119–128.

990 7. Abad A, Victoria Fernández-Molina J, Bikandi J, Ramírez A, Margareto J,
991 Sendino J, Luis Hernando F, Pontón J, Garaizar J, Rementeria A. 2010.
992 ¿Qué hace que Aspergillus fumigatus sea un patógeno de éxito? Genes y
993 moléculas involucrados en la aspergilosis invasora. Rev Iberoam Micol
994 27:155–182.

995 8. Lee IR, Yang L, Sebetso G, Allen R, Doan THN, Blundell R, Lui EYL,
996 Morrow CA, Fraser JA. 2013. Characterization of the Complete Uric Acid
997 Degradation Pathway in the Fungal Pathogen Cryptococcus neoformans.
998 PLoS One 8:1–13.

999 9. Rüping MJGT, Vehreschild JJ, Cornely OA. 2008. Patients at High Risk of
1000 Invasive Fungal Infections. Drugs 68:1941–1962.

1001 10. Guinea J, Torres-Narbona M, Gijón P, Muñoz P, Pozo F, Peláez T, de
1002 Miguel J, Bouza E. 2010. Pulmonary aspergillosis in patients with chronic
1003 obstructive pulmonary disease: Incidence, risk factors, and outcome. Clin
1004 Microbiol Infect 16:870–877.

1005 11. Gonçalves SS, Souza ACR, Chowdhary A, Meis JF, Colombo AL. 2016.
1006 Epidemiology and molecular mechanisms of antifungal resistance
1007 in Candida and Aspergillus. Mycoses 59:198–219.

1008 12. Rudramurthy SM, Paul RA, Chakrabarti A, Mouton JW, Meis JF. 2019.
1009 Invasive aspergillosis by aspergillus flavus: Epidemiology, diagnosis,
1010 antifungal resistance, and management. J Fungi 5:1–23.

1011 13. Patterson TF, Thompson GR, Denning DW, Fishman JA, Hadley S,
1012 Herbrecht R, Kontoyiannis DP, Marr KA, Morrison VA, Nguyen MH, Segal
1013 BH, Steinbach WJ, Stevens DA, Walsh TJ, Wingard JR, Young JAH,
1014 Bennett JE. 2016. Executive summary: Practice guidelines for the

diagnosis and management of aspergillosis: 2016 update by the infectious diseases society of America. Clin Infect Dis 63:433–442.

14. Perlin DS, Rautemaa-Richardson R, Alastruey-Izquierdo A. 2017. The global problem of antifungal resistance: prevalence, mechanisms, and management. Lancet Infect Dis 17:e383–e392.

15. Alastruey-Izquierdo A, Cadranel J, Flick H, Godet C, Hennequin C, Hoenigl M, Kosmidis C, Lange C, Munteanu O, Page I, Salzer HJF. 2018. Treatment of Chronic Pulmonary Aspergillosis: Current Standards and Future Perspectives. Respiration 96:159–170.

16. Denning DW, Cadranel J, Beigelman-Aubry C, Ader F, Chakrabarti A, Blot S, Ullmann AJ, Dimopoulos G, Lange C. 2016. Chronic pulmonary aspergillosis: Rationale and clinical guidelines for diagnosis and management. Eur Respir J 47:45–68.

17. Latgé, Jean-Paul ; Chamilos G. 2020. Aspergillus fumigatus and Aspergillosis in 2019. Clin Microbiol Rev 33:1–75.

18. Tekaia F, Latgé JP. 2005. Aspergillus fumigatus: Saprophyte or pathogen? Curr Opin Microbiol 8:385–392.

19. Agarwal R, Chakrabarti A, Shah A, Gupta D, Meis JF, Guleria R, Moss R, Denning DW. 2013. Allergic bronchopulmonary aspergillosis: Review of literature and proposal of new diagnostic and classification criteria. Clin Exp Allergy 43:850–873.

20. Van De Veerdonk FL, Gresnigt MS, Romani L, Netea MG, Latgé JP. 2017. Aspergillus fumigatus morphology and dynamic host interactions. Nat Rev Microbiol 15:661–674.

21. Gergen PJ, Arbes SJ, Calatroni A, Mitchell HE, Zeldin DC. 2009. Total IgE levels and asthma prevalence in the US population: Results from the National Health and Nutrition Examination Survey 2005-2006. J Allergy Clin Immunol 124:447–453.

22. Vacher G, Niculita-Hirzel H, Roger T. 2015. Immune responses to airborne fungi and non-invasive airway diseases. Semin Immunopathol

37:83–96.

23. Kosmidis C, Denning DW. 2015. The clinical spectrum of pulmonary aspergillosis. Thorax 70:270–277.

24. Azie N, Neofytos D, Pfaller M, Meier-Kriesche HU, Quan SP, Horn D. 2012. The PATH (Prospective Antifungal Therapy) Alliance® registry and invasive fungal infections: Update 2012. Diagn Microbiol Infect Dis 73:293–300.

25. Almyroudis NG, Holland SM, Segal BH. 2005. Invasive aspergillosis in primary immunodeficiencies. Med Mycol 43:247–259.

26. Nett JE, Andes DR. 2016. Antifungal Agents: Spectrum of Activity, Pharmacology, and Clinical Indications. Infect Dis Clin North Am 30:51–83.

27. Holt SL, Drew RH. 2011. Echinocandins: Addressing outstanding questions surrounding treatment of invasive fungal infections. Am J Heal Pharm 68:1207–1220.

28. Perfect JR. 2017. The antifungal pipeline: A reality check. Nat Rev Drug Discov 16:603–616.

29. Allen D, Wilson D, Drew R, Perfect J. 2015. Azole antifungals: 35 years of invasive fungal infection management. Expert Rev Anti Infect Ther 13:787–798.

30. Denning DW, O'Driscoll BR, Hogaboam CM, Bowyer P, Niven RM. 2006. The link between fungi and severe asthma: A summary of the evidence. Eur Respir J 27:615–626.

31. Fontaine T, Delangle A, Simenel C, Coddeville B, van Vliet SJ, van Kooyk Y, Bozza S, Moretti S, Schwarz F, Trichot C, Aebi M, Delepierre M, Elbim C, Romani L, Latgé JP. 2011. Galactosaminogalactan, a new immunosuppressive polysaccharide of Aspergillus fumigatus. PLoS Pathog 7.

32. Hanadate T, Wakasugi M, Sogabe K, Kobayashi T, Horita H, Kawamura I, Hori Y, Matsui K, Hoshino Y, Sou M. 2011. Evaluation of the safety and

efficacy of micafungin in Japanese patients with deep mycosis: A post-marketing survey report. J Infect Chemother 17:622–632.

33. Walsh, Thomas J Elias J. Anaissie 2, David W. Denning 13, Raoul Herbrecht, 14 Dimitrios P. Kontoyiannis 3, Kieren A. Marr, 5 Vicki A. Morrison, 6 7, Brahm H Segal 8, William J. Steinbach 9, David A. Stevens, 10 11, Jo-Anne van Burik, 7 John R. Wingard 12, Patterson4 and TF, Tang XD, Li GH. 2008. Treatment of aspergillosis: Clinical practice guidelines of Infectious Diseases Society of America. Chinese J Infect Chemother 8:161–166.

34. Maertens J, Raad I, Petrikkos G, Boogaerts M, Selleslag D, Petersen FB, Sable CA, Kartsonis NA, Ngai A, Taylor A, Patterson TF, Denning DW, Walsh TJ. 2004. Efficacy and Safety of Caspofungin for Treatment of Invasive Aspergillosis in Patients Refractory to or Intolerant of Conventional Antifungal Therapy. Clin Infect Dis 39:1563–1571.

35. Verweij PE, Lestrade PPA, Melchers WJG, Meis JF. 2016. Azole resistance surveillance in Aspergillus fumigatus: Beneficial or biased? J Antimicrob Chemother 71:2079–2082.

36. Maertens JA, Raad II, Marr KA, Patterson TF, Kontoyiannis DP, Cornely OA, Bow EJ, Rahav G, Neofytos D, Aoun M, Baddley JW, Giladi M, Heinz WJ, Herbrecht R, Hope W, Karthaus M, Lee DG, Lortholary O, Morrison VA, Oren I, Selleslag D, Shoham S, Thompson GR, Lee M, Maher RM, Schmitt-Hoffmann AH, Zeiher B, Ullmann AJ. 2016. Isavuconazole versus voriconazole for primary treatment of invasive mould disease caused by Aspergillus and other filamentous fungi (SECURE): A phase 3, randomised-controlled, non-inferiority trial. Lancet 387:760–769.

37. Miceli MH, Kauffman CA. 2015. Isavuconazole: A New Broad-Spectrum Triazole Antifungal Agent. Clin Infect Dis 61:1558–1565.

38. Tissot F, Agrawal S, Pagano L, Petrikkos G, Groll AH, Skiada A, Lass-Flörl C, Calandra T, Viscoli C, Herbrecht R. 2017. ECIL-6 guidelines for the treatment of invasive candidiasis, aspergillosis and mucormycosis in leukemia and hematopoietic stem cell transplant patients. Haematologica

102:433–444.

39. Ullmann AJ, Aguado JM, Arikan-Akdagli S, Denning DW, Groll AH, Lagrou K, Lass-Flörl C, Lewis RE, Munoz P, Verweij PE, Warris A, Ader F, Akova M, Arendrup MC, Barnes RA, Beigelman-Aubry C, Blot S, Bouza E, Brüggemann RJM, Buchheidt D, Cadranel J, Castagnola E, Chakrabarti A, Cuenca-Estrella M, Dimopoulos G, Fortun J, Gangneux JP, Garbino J, Heinz WJ, Herbrecht R, Heussel CP, Kibbler CC, Klimko N, Kullberg BJ, Lange C, Lehrnbecher T, Löffler J, Lortholary O, Maertens J, Marchetti O, Meis JF, Pagano L, Ribaud P, Richardson M, Roilides E, Ruhnke M, Sanguinetti M, Sheppard DC, Sinkó J, Skiada A, Vehreschild MJGT, Viscoli C, Cornely OA. 2018. Diagnosis and management of Aspergillus diseases: executive summary of the 2017 ESCMID-ECMM-ERS guideline. Clin Microbiol Infect 24:e1–e38.

40. Garcia-Rubio R, Cuenca-Estrella M, Mellado E. 2017. Triazole Resistance in Aspergillus Species: An Emerging Problem. Drugs 77:599–613.

41. Sharpe AR, Lagrou K, Meis JF, Chowdhary A, Lockhart SR, Verweij PE. 2018. Triazole resistance surveillance in Aspergillus fumigatus. Med Mycol 56:S83–S92.

42. Arikan-Akdagli S, Ghannoum M, Meis JF. 2018. Antifungal resistance: specific focus on multidrug resistance in candida auris and secondary azole resistance in aspergillus fumigatus. J Fungi 4:1–13.

43. Chen P, Liu J, Zeng M, Sang H. 2020. Exploring the molecular mechanism of azole resistance in Aspergillus fumigatus. J Mycol Med 30:100915.

44. Wiederhold NP, Verweij PE. 2020. Aspergillus fumigatus and pan-azole resistance: who should be concerned? Curr Opin Infect Dis 33:290–297.

45. Wiederhold NP. 2017. Antifungal resistance: current trends and future strategies to combat. Infect Drug Resist 10:249–259.

46. Snelders E, Van Der Lee HAL, Kuijpers J, Rijs AJMM, Varga J, Samson RA, Mellado E, Donders ART, Melchers WJG, Verweij PE. 2008.

1137 Emergence of azole resistance in Aspergillus fumigatus and spread of a
1138 single resistance mechanism. PLoS Med 5:1629–1637.

1139 47. Camps SMT, Rijs AJMM, Klaassen CHW, Meis JF, O'Gorman CM, Dyer
1140 PS, Melchers WJG, Verweij PE. 2012. Molecular epidemiology of
1141 Aspergillus fumigatus isolates harboring the TR34/L98H azole resistance
1142 mechanism. J Clin Microbiol 50:2674–2680.

1143 48. Meneau I, Sanglard D. 2005. Azole and fungicide resistance in clinical
1144 and environmental Aspergillus fumigatus isolates. Med Mycol 43:307–
1145 311.

1146 49. Toyotome T. 2019. Resistance in the environmental pathogenic fungus
1147 Aspergillus fumigatus. Med Mycol J 60:61–63.

1148 50. Blosser SJ, Cramer RA. 2012. SREBP-Dependent Triazole Susceptibility
1149 in Aspergillus fumigatus is Mediated through Direct Transcriptional
1150 Regulation of erg11A (cyp51A). Antimicrob Agents Chemother 56:248–
1151 257.

1152 51. Fraczek MG, Bromley M, Buied A, Moore CB, Rajendran R, Rautemaa R,
1153 Ramage G, Denning DW, Bowyer P. 2013. The cdr1B efflux transporter is
1154 associated with non- cyp51a -mediated itraconazole resistance in
1155 Aspergillus fumigatus. J Antimicrob Chemother Chemother 68:1486–
1156 1496.

1157 52. Buied A, Moore CB, Denning DW, Bowyer P. 2013. High-level expression
1158 of cyp51B in azole-resistant clinical Aspergillus fumigatus isolates. J
1159 Antimicrob Chemother 68:512–514.

1160 53. Rajendran R, Mowat E, Mcculloch E, Lappin DF, Jones B, Lang S,
1161 Majithiya JB, Warn P, Williams C, Ramage G. 2011. Azole Resistance of
1162 Aspergillus fumigatus Biofilms Is Partly Associated with Efflux Pump
1163 Activity. Antimicrob Agents Chemother 55:2092–2097.

1164 54. Hagiwara D, Watanabe A, Kamei K, Goldman GH. 2016. Epidemiological
1165 and genomic landscape of azole resistance mechanisms in Aspergillus
1166 fungi. Front Microbiol 7:1–14.

55. Hagiwara D, Watanabe A, Kamei K. 2016. Sensitisation of an Azole-Resistant Aspergillus fumigatus Strain containing the Cyp51A-Related Mutation by Deleting the SrbA Gene. Sci Rep 6:1–8.

56. Gonzalez-Lara MF, Roman-Montes CM, Diaz-Lomeli P, Rangel-Cordero A, Valenzuela MO, Ponce-De-Leon A, Sifuentes-Osornio J, Ostrosky-Zeichner L, Martinez-Gamboa A. 2019. Azole resistance and cyp51A mutation screening in Aspergillus fumigatus in Mexico. J Antimicrob Chemother 74:2047–2050.

57. Lestrade PPA, Meis JF, Melchers WJG, Verweij PE. 2019. Triazole resistance in Aspergillus fumigatus: recent insights and challenges for patient management. Clin Microbiol Infect 25:799–806.

58. Lass-Flörl C, Kofler G, Kropshofer G, Hermans J, Kreczy A, Dierich MP, Niederwieser D. 1998. In-vitro testing of susceptibility to amphotericin B is a reliable predictor of clinical outcome in invasive aspergillosis. J Antimicrob Chemother 42:497–502.

59. Hadrich I, Makni F, Neji S, Cheikhrouhou F, Bellaaj H, Elloumi M, Ayadi A, Ranque S. 2012. Amphotericin B in vitro resistance is associated with fatal Aspergillus flavus infection. Med Mycol 87:829–834.

60. Reichert-Lima F, Lyra L, Pontes L, Moretti ML, Pham CD, Lockhart SR, Schreiber AZ. 2018. Surveillance for azoles resistance in Aspergillus spp. highlights a high number of amphotericin B-resistant isolates. Mycoses 61:360–365.

61. Vahedi Shahandashti R, Lass-Flörl C. 2019. Antifungal resistance in Aspergillus terreus: A current scenario. Fungal Genet Biol 131:103247.

62. Oliver JD, Sibley GEM, Beckmann N, Dobb KS, Slater MJ, McEntee L, du Pré S, Livermore J, Bromley MJ, Wiederhold NP, Hope WW, Kennedy AJ, Law D, Birch M. 2016. F901318 represents a novel class of antifungal drug that inhibits dihydroorotate dehydrogenase. Proc Natl Acad Sci 113:12809–12814.

63. Moreno-Martinez E, Vallieres C, Holland SL, Avery S V. 2015. Novel, Synergistic Antifungal Combinations that Target Translation Fidelity. Sci

Rep 5:1–11.

64. Joffe LS, Schneider R, Lopes W, Azevedo R, Staats CC, Kmetzsch L, Schrank A, Poeta M Del, Vainstein MH, Rodrigues ML. 2017. The anti-helminthic compound mebendazole has multiple antifungal effects against Cryptococcus neoformans. Front Microbiol 8:1–14.

65. Nicola Nosengo. 2016. Can you teach old drugs new tricks? Nature 534:314–316.

66. Kaul G, Shukla M, Dasgupta A, Chopra S. 2019. Update on drug-repurposing: Is it useful for tackling antimicrobial resistance? Future Microbiol 14:829–831.

67. Rhein J, Morawski BM, Hullsiek KH, Nabeta HW, Kiggundu R, Tugume L, Musubire A, Akampurira A, Smith KD, Alhadab A, Williams DA, Abassi M, Bahr NC, Velamakanni SS, Fisher J, Nielsen K, Meya DB, Boulware DR, Ndyetukira JF, Ahimbisibwe C, Kugonza F, Sadiq A, Kandole TK, Luggya T, Kaboggoza J, Laker E, Butler EK, Dyal J, Neborak JM, King AM, Fujita AW, Yueh N, Namudde A, Halupnick R, Jawed B, Vedula P, Peterson M, Bohjanen PR, Kambugu A. 2016. Efficacy of adjunctive sertraline for the treatment of HIV-associated cryptococcal meningitis: An open-label dose-ranging study. Lancet Infect Dis 16:809–818.

68. Duffy S, Sykes ML, Jones AJ, Shelper TB, Simpson M, Lang R, Poulsen SA, Sleebs BE, Avery VM. 2017. Screening the medicines for malaria venture pathogen box across multiple pathogens reclassifies starting points for open-source drug discovery. Antimicrob Agents Chemother 61.

69. Hennessey KM, Rogiers IC, Shih HW, Hulverson MA, Choi R, McCloskey MC, Whitman GR, Barrett LK, Merritt EA, Paredez AR, Ojo KK. 2018. Screening of the Pathogen Box for inhibitors with dual efficacy against Giardia lamblia and Cryptosporidium parvum. PLoS Negl Trop Dis 12:1–16.

70. Spalenka J, Sandie Escotte-Binet, Ali Bakiri, Jane Hubert, Jean-Hugues Renault, Frédéric Velard, Simon Duchateau, Dominique Aubert, Antoine Huguenin IV. 2018. crossm Discovery of New Inhibitors of Toxoplasma

gondii via the 62:1–10.

71. Wall G, Herrera N, Lopez-Ribot JL. 2019. Repositionable compounds with antifungal activity against multidrug resistant candida auris identified in the medicines for malaria venture's pathogen box. J Fungi 5.

72. Dorlo TPC, Balasegaram M, Beijnen JH, de vries PJ. 2012. Miltefosine: A review of its pharmacology and therapeutic efficacy in the treatment of leishmaniasis. J Antimicrob Chemother 67:2576–2597.

73. Sundar S. 2009. An Update on Pharmacotherapy for Leishmaniasis Shyam 16:186–189.

74. Simm C, May RC. 2019. Zinc and Iron Homeostasis : Target-Based Drug Screening as New Route for Antifungal Drug Development. Front Cell Infect Microbiol 9:1–12.

75. Santos JRA, Gouveia LF, Taylor ELS, Resende-Stoianoff MA, Pianetti GA, César IC, Santos DA. 2012. Dynamic Interaction between Fluconazole and Amphotericin B against Cryptococcus gattii. Antimicrob Agents Chemother 56:2553–2558.

76. Odds FC. 2003. Synergy , antagonism , and what the chequerboard puts between them. J Antimicrob Chemother 52:273144.

77. Armitage EG, Alqaisi AQI, Godzien J, Peña I, Mbekeani AJ, Alonso-Herranz V, López-Gonzálvez Á, Martín J, Gabarro R, Denny PW, Barrett MP, Barbas C. 2018. Complex interplay between sphingolipid and sterol metabolism revealed by perturbations to the leishmania metabolome caused by miltefosine. Antimicrob Agents Chemother 62:1–12.

78. Pinto-Martinez AK, Rodriguez-Durán J, Serrano-Martin X, Hernandez-Rodriguez V, Benaim G. 2018. Mechanism of action of miltefosine on Leishmania donovani involves the impairment of acidocalcisome function and the activation of the sphingosine-dependent plasma membrane Ca 2+ channel. Antimicrob Agents Chemother 62:1–10.

79. Miyake Y, Kozutsumi Y, Nakamura S, Fujita T, Kawasaki T. 1995. Serine palmitoyltransferase is 735 the primary target of a sphingosine-like

immunosuppressant, ISP-1/myriocin. Biochem Biophys Res Commun 211.

80. Furukawa T, van Rhijn N, Fraczek M, Gsaller F, Davies E, Carr P, Gago S, Fortune-Grant R, Rahman S, Gilsenan JM, Houlder E, Kowalski CH, Raj S, Paul S, Cook P, Parker JE, Kelly S, Cramer RA, Latgé JP, Moye-Rowley S, Bignell E, Bowyer P, Bromley MJ. 2020. The negative cofactor 2 complex is a key regulator of drug resistance in Aspergillus fumigatus. Nat Commun 11.

81. Ukil L, Varadaraj A, Govindaraghavan M, Liu HL, Osmani SA. 2008. Copy number suppressors of the Aspergillus nidulans nimA1 mitotic kinase display distinctive and highly dynamic cell cycle-regulated locations. Eukaryot Cell 7:2087–2099.

82. Bertuzzi M, Schrettl M, Alcazar-Fuoli L, Cairns TC, Muñoz A, Walker LA, Herbst S, Safari M, Cheverton AM, Chen D, Liu H, Saijo S, Fedorova ND, Armstrong-James D, Munro CA, Read ND, Filler SG, Espeso EA, Nierman WC, Haas H, Bignell EM. 2014. The pH-Responsive PacC Transcription Factor of Aspergillus fumigatus Governs Epithelial Entry and Tissue Invasion during Pulmonary Aspergillosis. PLoS Pathog 10.

83. Dinamarco TM, Almeida RS, de Castro PA, Brown NA, dos Reis TF, Ramalho LNZ, Savoldi M, Goldman MHS, Goldman GH. 2012. Molecular characterization of the putative transcription factor SebA involved in virulence in Aspergillus fumigatus. Eukaryot Cell 11.

84. Neubauer M, Zhu Z, Penka M, Helmschrott C, Wagener N, Wagener J. 2015. Mitochondrial dynamics in the pathogenic mold Aspergillus fumigatus: Therapeutic and evolutionary implications. Mol Microbiol 98:930–945.

85. Ruf D, Brantl V, Wagener J. 2018. Mitochondrial fragmentation in Aspergillus fumigatus as early marker of granulocyte killing activity. Front Cell Infect Microbiol 8.

86. Hornillos V, Carrillo E, Rivas L, Amat-Guerri F, Acuña AU. 2008. Synthesis of BODIPY-labeled alkylphosphocholines with leishmanicidal

activity, as fluorescent analogues of miltefosine. Bioorganic Med Chem Lett 18:6336–6339.

87. Nakahara K, Ohkuni A, Kitamura T, Abe K, Naganuma T, Ohno Y, Zoeller RA, Kihara A. 2012. The Sjögren-Larsson Syndrome Gene Encodes a Hexadecenal Dehydrogenase of the Sphingosine 1-Phosphate Degradation Pathway. Mol Cell 46:461–471.

88. Bastos RW, Rossato L, Valero C, Lagrou K, Colombo AL, Goldman GH. 2019. Potential of Gallium as an Antifungal Agent. Front Cell Infect Microbiol 9:1–11.

89. Riat A, Plojoux J, Gindro K, Schrenzel J. 2018. Azole Resistance of Environmental and Clinical Aspergillus. Antimicrob Agents Chemother 62:1–7.

90. Colombo AL, de Almeida Júnior JN, Slavin MA, Chen SCA, Sorrell TC. 2017. Candida and invasive mould diseases in non-neutropenic critically ill patients and patients with haematological cancer. Lancet Infect Dis 17:e344–e356.

91. Mayer FL, Kronstad JW. 2017. Discovery of a Novel Antifungal Agent in the Pathogen Box. mSphere 2:1–12.

92. Scorneaux B, Angulo D, Borroto-esoda K. 2017. SCY-078 Is Fungicidal against Candida Species in time-kill studies. Antimicrob Agents Chemother 61:1–10.

93. Vallières C, Avery S. 2017. The Candidate Antimalarial Drug MMV665909 Causes Oxygen-Dependent mRNA Mistranslation and Synergizes with Quinoline-Derived Antimalarials. Antimicrob Agents Chemother 61:1–11.

94. Eibl H, Ungert C. 1990. Hexadecylphosphocholine : a new and selective antitumor drug. Cancer Trmtnent Rev 17:233–242.

95. Croft SL, Snowdon D, Yardley V. 1996. The activities of four anticancer alkyllysophospholipids against Leishmania donovani , Trypanosoma cruzi and Trypanosoma brucei. J Antimicrob Chemother 38:1041–1047.

96. Urbina JA. 2006. Mechanisms of action of lysophospholipid analogues

against trypanosomatid parasites. Trans R Soc Trop Med Hyg 100S:S9–S16.

97. Díaz Y de las MZ, Ambroggio EE, Fanani ML. 2020. Miltefosine inhibits the membrane remodeling caused by phospholipase action by changing membrane physical properties. BBA - Biomembr 183407.

98. Luque-Ortega J, Rivas L. 2007. Miltefosine (Hexadecylphosphocholine) Inhibits Cytochrome c Oxidase in Leishmania donovani Promastigotes □. Antimicrob Agents Chemother 51:1327–1332.

99. Bhattacharya A, Leprohon P, Bigot S, Padmanabhan PK, Mukherjee A, Roy G, Gingras H, Mestdagh A, Papadopoulou B, Ouellette M. 2019. Coupling chemical mutagenesis to next generation sequencing for the identification of drug resistance mutations in Leishmania. Nat Commun 10.

100. Borba-Santos LP, Gagini T, Ishida K, De Souza W, Rozental S. 2015. Miltefosine is active against sporothrix brasiliensis isolates with in vitro low susceptibility to amphotericin B or itraconazole. J Med Microbiol 64:415–422.

101. Brilhante RSN, Malaquias ÂDM, Caetano ÉP, De Souza Collares Maia Castelo-Branco D, De Lima RAC, De Farias Marques FJ, Silva NF, De Alencar LP, Monteiro AJ, De Camargo ZP, De Jesus Pinheiro Gomes Bandeira T, Rodrigues AM, De Aguiar Cordeiro R, Moreira JLB, Sidrim JJC, Rocha MFG. 2014. In vitro inhibitory effect of miltefosine against strains of Histoplasma capsulatum var. capsulatum and Sporothrix spp. Med Mycol 52:320–325.

102. Barreto TL, Rossato L, de Freitas ALD, Meis JF, Lopes LB, Colombo AL, Ishida K. 2020. Miltefosine as an alternative strategy in the treatment of the emerging fungus Candida auris. Int J Antimicrob Agents 56.

103. Imbert S, Palous M, Meyer I, Dannaoui E, Mazier D, Datry A, Fekkar A. 2014. In vitro combination of voriconazole and miltefosine against clinically relevant molds. Antimicrob Agents Chemother 58:6996–6998.

104. Rossi DCP, Spadari C de C, Nosanchuk JD, Taborda CP, Ishida K. 2017.

Miltefosine is fungicidal to Paracoccidioides spp. yeast cells but subinhibitory concentrations induce melanisation. Int J Antimicrob Agents 49:465–471.

105. Spadari C de C, Vila T, Rozental S, Ishida K. 2018. Miltefosine has a postantifungal effect and induces apoptosis in cryptococcus yeasts. Antimicrob Agents Chemother 62.

106. Spadari C de C, de Bastiani FWM da S, Lopes LB, Ishida K. 2019. Alginate nanoparticles as non-toxic delivery system for miltefosine in the treatment of candidiasis and cryptococcosis. Int J Nanomedicine 14:5187–5199.

107. de Bastiani FWM da S, Spadari C de C, de Matos JKR, Salata GC, Lopes LB, Ishida K. 2020. Nanocarriers Provide Sustained Antifungal Activity for Amphotericin B and Miltefosine in the Topical Treatment of Murine Vaginal Candidiasis. Front Microbiol 10:1–9.

108. Vila TVM, Chaturvedi AK, Rozental S, Lopez-Ribot JL. 2015. In vitro activity of miltefosine against Candida albicans under planktonic and biofilm growth conditions and in vivo efficacy in a murine model of oral candidiasis. Antimicrob Agents Chemother 59:7611–7620.

109. Widmer F, Wright LC, Obando D, Handke R, Ganendren R, Ellis DH, Sorrell TC. 2006. Hexadecylphosphocholine (miltefosine) has broad-spectrum fungicidal activity and is efficacious in a mouse model of cryptococcosis. Antimicrob Agents Chemother 50:414–421.

110. Wu Y, Wu M, Gao J, Ying C. 2020. Antifungal Activity and Mode of Action of Miltefosine Against Clinical Isolates of Candida krusei. Front Microbiol 11:1–8.

111. Wu Y, Totten M, Memon W, Ying C, Zhang SX. 2020. In Vitro Antifungal Susceptibility of the Emerging Multidrug- Resistant Pathogen Candida auris to Miltefosine Alone and in Combination with Amphotericin B. Antimicrob Agents Chemother 64.

112. Dorlo TPC, Balasegaram M, Beijnen JH, de vries PJ. 2012. Miltefosine: A review of its pharmacology and therapeutic efficacy in the treatment of

leishmaniasis. J Antimicrob Chemother 67:2576–2597.

113. Zuo X, Djordjevic JT, Oei JB, Desmarini D, Schibeci SD, Jolliffe KA, Sorrell TC. 2011. Miltefosine induces apoptosis-like cell death in yeast via Cox9p in cytochrome c oxidase. Mol Pharmacol 80:476–485.

114. Compain F, Botterel F, Sitterl E, Paugam A, Bougnoux ME, Dannaoui E. 2015. In vitro activity of miltefosine in combination with voriconazole or amphotericin B against clinical isolates of scedosporium spp. J Med Microbiol 64:309–311.

115. Maertens JA. 2004. History of the development of azole derivatives. Clin Microbiol Infect Suppl 10:1–10.

116. Anderson TM, Clay MC, Cioffi AG, Diaz KA, Hisao GS, Tuttle MD, Nieuwkoop AJ, Comellas G, Maryum N, Wang S, Uno BE, Wildeman EL, Gonen T, Rienstra CM, Burke MD. 2014. amphotericin forms an extramembranous and fungicidal sterol sponge. Nat Chem Biol 10.

117. Robbins N, Caplan T, Cowen LE. 2017. Molecular Evolution of Antifungal Drug Resistance. Annu Rev ofMicrobiology 71:753–775.

118. Biswas C, Sorrell TC, Djordjevic JT, Zuo X, Jolliffe KA, Chen SCA. 2013. In vitro activity of miltefosine as a single agent and in combination with voriconazole or posaconazole against uncommon filamentous fungal pathogens. J Antimicrob Chemother 68:2842–2846.

119. Dickson RC, Sumanasekera C, Lester RL. 2006. Functions and metabolism of sphingolipids in Saccharomyces cerevisiae. Prog Lipid Res 45:447–465.

120. Cheng J, Park T-S, Fischl AS, Ye XS. 2001. Cell Cycle Progression and Cell Polarity Require Sphingolipid Biosynthesis in Aspergillus nidulans. Mol Cell Biol 21:6198–6209.

121. Heung LJ, Luberto C, Poeta M Del. 2006. Role of Sphingolipids in Microbial Pathogenesis. Infect Immun 74:28–39.

122. Rella A, Farnoud AM, Poeta M Del. 2016. Plasma membrane lipids and their role in fungal virulence. Prog Lipid Res 61:63–72.

123. Cheng J, Park T, Chio L, Fischl AS, Ye XS. 2003. Induction of Apoptosis by Sphingoid Long-Chain Bases in Aspergillus nidulans. Mol Cell Biol 23:163–177.

124. Käfer E. 1977. Meiotic and Mitotic Recombination in Aspergillus and Its Chromosomal Aberrations, p. 33–131. *In* Advances in Genetics.

125. CLSI. 2008. Reference Method for Broth Dilution.

126. Goméz-Lopes A, Cuenca-estrella M, Mellado E, Rodrígez-Tudela JL. 2003. In vitro evaluation of combination of terbinafine with itraconazole or amphotericin B against Zygomycota. Diagn Microbiol Infect Dis 45:199–202.

127. Colot H V, Park G, Turner GE, Ringelberg C, Crew CM, Litvinkova L, Weiss RL, Borkovich KA, Dunlap JC. 2006. A high-throughput gene knockout procedure for Neurospora reveals functions for multiple transcription factors. PNAS 103.

128. Semighini CP, Marins M, Goldman MHS, Goldman GH. 2002. Quantitative Analysis of the Relative Transcript Levels of ABC Transporter Atr Genes in Aspergillus nidulans by Real-Time Reverse Transcription-PCR Assay. Appl Environ Microbiol 68:1351–1357.

129. Fan X, Lamarre-vincent N, Wang Q, Struhl K. 2008. Extensive chromatin fragmentation improves enrichment of protein binding sites in chromatin immunoprecipitation experiments. Nucleic Acids Res 36:1–7.

130. Wong KH, Struhl K. 2011. The Cyc8 – Tup1 complex inhibits transcription primarily by masking the activation domain of the recruiting protein. Genes Dev 25:2525–2539.

131. Langmead B, Trapnell C, Pop M, Salzberg SL. 2009. Ultrafast and memory-efficient alignment of short DNA sequences to the human genome. Genome Biol 10.

132. Singh A, Poeta M Del. 2016. Sphingolipidomics : An Important Mechanistic Tool for Studying Fungal Pathogens. Front Microbiol 7:1–14.

133. Singh A, Mackenzie A, Girnun G, Poeta M Del. 2017. Analysis of

sphingolipids , sterols , and phospholipids in human pathogenic Cryptococcus strains. J Lipid Res 58:2017–2036.

134. Mandala SM, Thornton RA, Frommer BR, Curotto JE, Rozdilsky W, Kurtz MB, Giacobbe RA, Bills GF, Cabello MA, Martin I, Pelaez F, Harris GH. 1995. The Discovery of Australifungin , a Novel Inhibitor of Sphinganine TV-Acyltransferase from Sporormiella australis Producing Organism , Fermentation , Isolation , and Biological Activity. J Antibiot (Tokyo) 48.

135. Bligh E, Dyer W. 1959. A rapid method of total lipid extraction and purification. Can J Biochem Physiol 37.

136. Clarke NG, Dawson RM. 1981. Alkaline O-N-transacylation: A new method for the quantitative deacylation of phospholipids Neville. Biochem J 195:301–306.

137. Jemel S, Guillot J, Kallel K, Botterel F, Dannaoui E. 2020. Galleria mellonella for the evaluation of antifungal efficacy against medically important fungi, a narrative review. Microorganisms 8.

138. Fernandes C, Fonseca F, Goldman G, Pereira M, Kurtenbach E. 2017. A Reliable Assay to Evaluate the Virulence of Aspergillus nidulans Using the Alternative Animal Model Galleria mellonella (Lepidoptera). Bio-Protocol 7:1–13.

139. Heel RC, Morton P, Brogden RN, Speight TM, Avery GS. 1979. Econazole: A Review of its Antifungal Activity and Therapeutic Efficacy. Drugs 18:177–201.

140. Tavakkoli A, Johnston TP, Sahebkar A. 2020. Antifungal effects of statins. Pharmacol Ther 208:107483.

141. Su Z, Martin R, Cox BF, Gintant G. 2004. Mesoridazine: An open-channel blocker of human ether-a-go-go-related gene K+ channel. J Mol Cell Cardiol 36:151–160.

142. Orihata M, Sarna SK. 1994. Contractile mechanisms of action of gastroprokinetic agents: Cisapride, metoclopramide, and domperidone. Am J Physiol - Gastrointest Liver Physiol 266:665–676.

143. Del Rosso JQ, Kircik LH. 2013. Optimizing topical antifungal therapy for superficial cutaneous fungal infections: focus on topical naftifine for cutaneous dermatophytosis. J drugs dermatology 12:165–171.

144. Pollak EB, Parmar M. 2021. IndinavirStatPearls.

145. Davies R, Gomez H, Irvin J, Walker J. 1984. An overview of the clinical pharmacology of enalapril. Br J Clin Pharmacol 18:215S-229S.

146. Franzyk H, Christensen SB. 2021. Targeting Toxins toward Tumors. Molecules 26.

147. Gupta YK, Gupta M, Aneja S, Kohli K. 2004. Current Drug Therapy of Protozoal Diarrhoea. Indian J Pediatr 71:55–58.

148. Roatt BM, de Oliveira Cardoso JM, De Brito RCF, Coura-Vital W, de Oliveira Aguiar-Soares RD, Reis AB. 2020. Recent advances and new strategies on leishmaniasis treatment. Appl Microbiol Biotechnol 104:8965–8977.

Figure Legends

Figure 1. Miltefosine is a potential new anti-aspergillosis compound and shows its interaction with the sphingolipid inhibitor myriocin. (A). Screening of chemical libraries reveals potential new anti-aspergilosis compounds. (B) Interaction between miltefosine and Posaconazole. (C) Interaction between miltefosine and voriconazole. (D) Interaction between miltefosine and amphotericin B. (E) Interaction between miltefosine and caspofungin. (F) Interaction between miltefosine and myriocin

Figure 2. Radial growth of transcription factor (TF) null mutants in presence of miltefosine. (A) A total of 1 x 10^5 conidia of each specie was inoculated on MM supplemented or not with increasing concentration of miltefosine. Plates were incubated for 3 days at 37°C. (B) Quantification of the results obtained in (A). For each strain three independent experiments were realized and the graphic shows the mean ± standard deviations.

Figure 3. Molecular characterization of *rmiA*. (A) Growth phenotypes of the wild-type, Δ*rmiA* and Δ*rmiA::rmiA*$^{+}$ strains grown for 3 days on solid MM supplemented with increasing concentrations of miltefosine. (B) Graphical quantification of fungal growth presented in (A). The results are the average of three repetitions ± standard deviation of three repetitions. (C) RmiA:GFP translocates to the nucleus under exposure to miltefosine. (D) Graphical quantification of RmiA:GFP location shown in (C). The results are the average of three repetitions ± standard deviation of 30 germlings for each repetition. (E) Western blotting assay showing the RmiA:HA expression after 0, 4 and 8h of incubation with 12.5 µg/mL miltefosine. Anti-HA antibody was used to detect the recombinant protein. Anti-actin antibody was used as a loading control. Statistical analysis was performed using one-tailed, paired *t* tests for comparisons to the control condition (*, p <0.05; ***,p< 0.001;)

Figure 4. There is increased mitochondrial fragmentation and cell death when *A. fumigatus* Δ*rmiA* is exposed to miltefosine. (A) Mitochondrial morphology revealed by mitotracker in the wild-type, Δ*rmiA*, and Δ*rmiA::rmiA*$^{+}$ strains. (B) Quantification of the mitochondrial fragmentation in the absence (control) and presence of miltefosine. (C) Quantification of PI^{+} (propidium iodide) germlings in the absence (control) and presence of miltefosine. The results are the average of three repetitions ± standard deviation of 30 germlings for each repetition.

Figure 5. The fluorescent miltefosine analogue MT-11C-BDP is localized in the mitochondria. (A) and (B) *A. fumigatus* germlings (16 h growth in MM) were exposed for 5 minutes to µg/mL of MT-11C-BDP. Germlings were stained with MitoTracker Deep Red^{TM} FM.

Figure 6. Transcriptional profiling of *A. fumigatus* wild-type and *ΔrmiA* exposed to miltefosine. (A) FunCat categorization of differently expressed genes (DEGs) up- and downregulated in the wild-type strain exposed to miltefosine in comparison to the wild-type strain grown in VMM (control). (B) FunCat analysis of DEGs downregulated in the Δ*rmiA* strain under miltefosine

exposure in comparison to the Δ*rmiA* grown in VMM. (C) Heat map of log2 fold change (Log2FC) of DEGs as determined by RNAseq. Log_2FC values are based on comparisons between (i) wild-type strain exposed to miltefosine *versus* wild-type strain in grown in MM (control); (ii) Δ*rmiA* grown in VMM (control) *versus* wild-type grown in VMM (control); (iii)) Δ*rmiA* strain exposed to miltefosine *versus* wild-type strain under miltefosine treatment. Hierarchical clustering was performed in Multiple Experiment Viewer (MeV) (http://mev.tm4.org/), using Pearson correlation with complete linkage clustering. Heat map scale and gene identities are shown. (D) Validation of RNA -seq data. Expression of three genes as determined by qRT -PCR after 0 and 30 minutes of exposition to 3µg/mL of miltefosine. Gene expression values were normalized by the expression of β-tubulin. Standard deviations are shown for biological triplicates.

Figure 7. Chromatin Immunoprecipitation coupled to next generation sequencing (ChIP-Seq) of the wild-type and the Δ*rmiA* strains exposed to miltefosine. (A) ChIP-Seq Integrative Genomics Viewer (IGV; http://software.broadinstitute.org/software/igv/download) screenshot for promoter regions of genes that bound to RmiA:3xHA when grown for 24 h in VMM or after the addition of 12.5 µg/mL miltefosine for 30 min. (B) Heat map of the ChIP-seq results for 6 genes showing the fold enrichment of RmiA binding after 0 and 30 minutes of exposure to 12.5 µg/mL of miltefosine and the RNAseq results for the same 6 genes in the WT and Δ*rmiA* strains after exposure to 3µg/mL during 30 minutes. (C) MEME (Multiple EM for Motif Elicitation)-ChIP analysis of the 500 bp region surrounding the peaks identified in the ChIP-seq analysis.

Figure 8. Deletion of *rmiA* leads to an overall reduction of sphingolipids biosynthesis in *A. fumigatus.* (A) The wild-type and Δ*rmiA* strains were grown in liquid VMM 16h and transferred to RPMI medium supplemented (or not) with 3 µg/mL miltefosine for additional 4h, the sphingolipids were extracted and measured by mass spectrometry. Heat maps labeled surrounded by boxes with gray borders represents the intermediates of SL biosynthetic pathwayheat maps surrounded by boxes with green borders represents the intermediates from the neutral branching while heat maps surrounded by boxes with yellow borders

represents the intermediates from the acidic branch of SL biosynthetic pathway. Heat maps show the values obtained by the ratio VMM/RPMI. Experiments were performed by using three independent biological experiments and the results are the average of them. Statistical analysis was performed using Student's t-test ($p<0.05$). (B) Diagram showing the different genes involved in the sphingolipids biosynthesis. Expression levels of genes encoding enzymes involved in the sphingolipids biosynthesis were selected from the RNAseq analysis. DHS, dihydrosphingosine; DHS-1P, dihydrosphingosine 1-phosphate; DHC, dihydroceramide; Cer, ceramide; GlcCer, glucosylceramide; OH-Cer, hydroxy-ceramide; PHS, phytosphingosine; PHS-1P, phytosphingosine 1-phosphate; PCer, phytoceramide; OH-PCer, hydroxy-phytoceramide; IPC, inositolphosphoryl ceramide.

Supplemental material

Supplementary Figure S1. The deletion of *rmiA* causes no growth impact in the presence of different stress conditions. Strains were grown from 10^5 spores for 5 days at 37°C on minimal media (MM) supplemented or not with (A) CaCl2, (B) calcofluor white (CFW), (C) sorbitol, (D) NaCl, (E) menadione and (F) variable temperature. The results are expressed as the average of radial diameter of the treatment divided by the radial diameter of the control of three independent experiments ± SD. Standard deviations present the average of three independent biological repetitions.

Supplementary Figure S2. Construction of *rmiA::3xHA* and *rmiA::GFP* strains. Both strains were constructed in the Δ*rmiA* background and confirmed by PCR sing *rmiA pRS426 3R* (P5) and *rmiA 1500UP ext F* (P6) primers. The *rmiA::3xHA* (A) and *rmiA::GFP* (B) are functional, do not present growth defects and restored the miltefosine sensitivity of the Δ*rmiA* null mutant.

Supplementary Table S1. Genes differentiallly expressed in the wild-type exposed to miltefosine.

Supplementary Table S2. Genes differentiallly expressed in the Δ*rmiA* mutant compared to the wild-type exposed to miltefosine.

Supplementary Table S3. Genes identified in the RmiA ChIP-seq.

Supplementary Table S4. Strains used in this work.

Supplementary Table S5. List of primers used in this work

Table 1. MIC values for NIH Clinical collection and Pathogen box compounds against *A. fumigatus*

	MIC (μM)	Description	Mode of Action	References
Econazole nitrate	12.5	broad-spectrum antimycotic agent	Inhibits ergosterol biosynthesis	(139)
Fluvastatin	25	statin drug class used for hypercholesterolemia treatment; the drug has demonstrated antifungal activity against some fungal species	blocks ergosterol biosynthesis by inhibition of farnesyl pyrophosphate production	(140)
Mesoridazine	3.12	piperidine neuroleptic drug used for the treatment of schizophrenia, organic brain disorders, alcoholism, and psychoneuroses	acts indirectly on reticular formation, whereby neuronal activity into reticular formation is reduced without affecting its intrinsic ability to activate the cerebral cortex	(141)
Cisapride	1.56	gastroprokinetic agent, a drug that increases motility in the upper gastrointestinal tract	Parasympathomimetic acting as a serotonin 5-HT_4 agonist	(142)
Oxiconazole nitrate	25	salt form of oxiconazole with antifungal activity	Inhibits ergosterol biosynthesis	(143)
Indinavir sulphate	6.25	antiretroviral protease inhibitor used in the therapy and prevention of human immunodeficiency virus (HIV) infection and the acquired immunodeficiency syndrome (AIDS)	Protease inhibitor	(144)
Enalaprilat	25	Used in the treatment of hypertension	Angiotensin-converting enzyme inhibitor	(145)

Vincristine sulfate	25	Used in cancer chemotherapy	Inhibits microtubule formation in mitotic spindle salt of a natural alkaloid with antimitotic and antineoplastic activities	(146)
Iodoquinol	2	antiprotozoal agent used as an amebicide drug	Unknown	(147)
Miltefosine	10	antiprotozoal, bactericidal and antifungal agent	Unknow	(148).

Table 2. Minimum inhibitory concentration (MIC, concentration in µg/µl) of *A. fumigatus* clinical isolates in the presence of different antifungals drugs

Strains	Itraconazole	Posaconazole	Voriconazole	Amphotericin B	Miltefosine
CEA17	2	2	1	0.5	4
F16134	>8	>8	4	0.25	4
F14946	>8	8	8	0.25	4
CYP15-117	>8	2	2	0.5	4
CYP15-147	>8	2	8	1	4
20089320	>8	4	4	1	4
CYP15-75	8	4	8	0.5	4
CYP15-91	8	1	2	1	4
CYP15-93	8	1	2	0.5	4
CYP15-106	8	2	1	1	4
CYP15-115	8	0.5	0.5	0.25	4
17993925	8	2	4	1	4
CYP15-109	4	1	>8	0.5	4
IF1S-F4	4	1	1	0.5	4
IFM59056	4	1	0.125	0.5	4
ISFT-021	2	1	0.25	1	4
IFM61407	2	2	0.125	0.5	4
MO68507	1	1	0.25	0.5	4
MO54056	1	1	0.125	0.5	4
IFM59056	1	1	0.125	0.5	4

A.

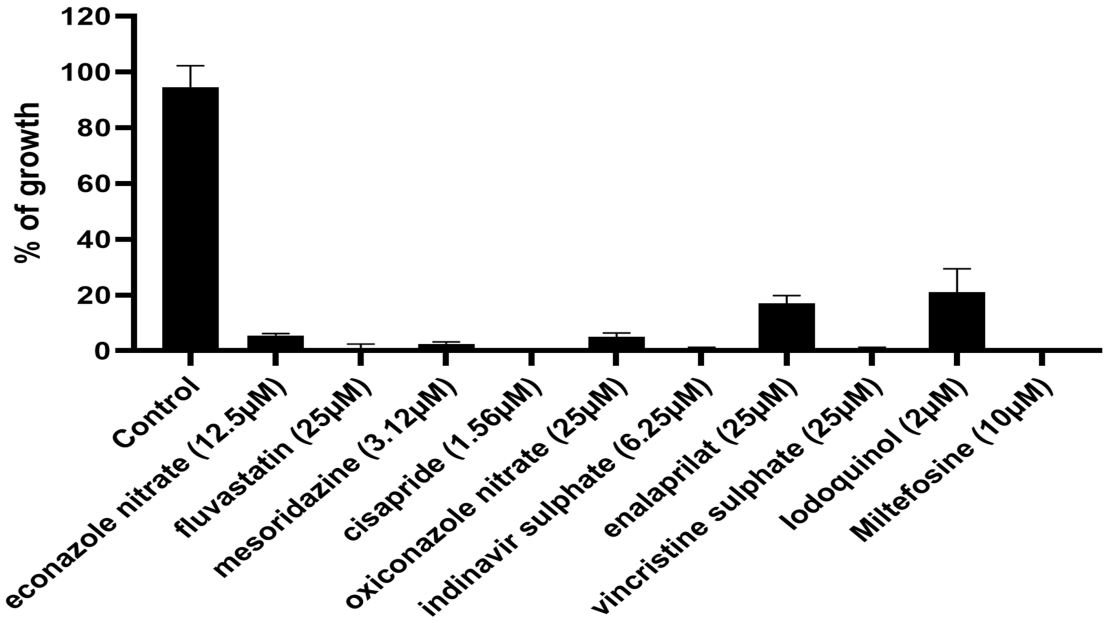

B.

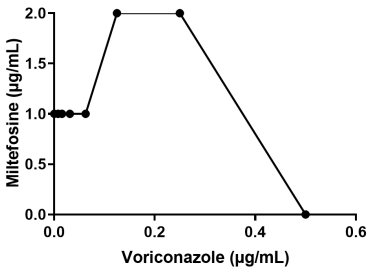

Drug	Voriconazole FICI (μg/mL)						
	0.007	0.015	0.031	0.062	0.125	0.25	Mean
Miltefosine	1.0	1.0	1.0	1.1	2.25	2.5	1.5

C.

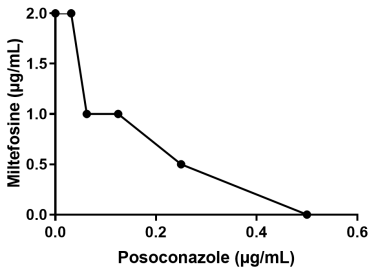

Drug	Posoconazole FICI (μg/mL)				
	0.031	0.062	0.125	0.25	Mean
Miltefosine	1.0	0.6	0.75	0.75	0.79

D.

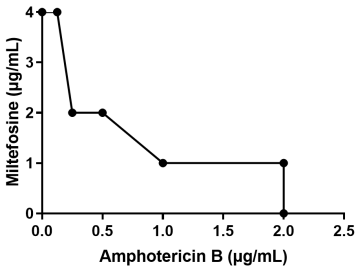

Drug	Amphotericin B FICI (μg/mL)					
	0.125	0.25	0.5	1.0	2.0	Mean
Miltefosine	1.0	0.6	0.7	0.7	1.2	0.9

E.

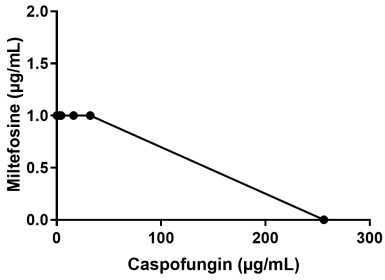

Drug	Caspofungin FICI (μg/mL)						
	1.0	2.0	4.0	8.0	16.0	32.0	Mean
Miltefosine	1.0	1.0	1.0	1.0	1.0	1.1	1.0

F.

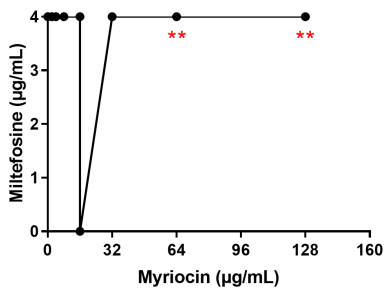

Drug	Myriocin FICI (μg/mL)							
	2.0	4.0	8.0	16.0	32.0	64.0	128	Mean
Miltefosine	1.1	1.2	1.5	2.0	3.0	5.0**	9.0**	3.2

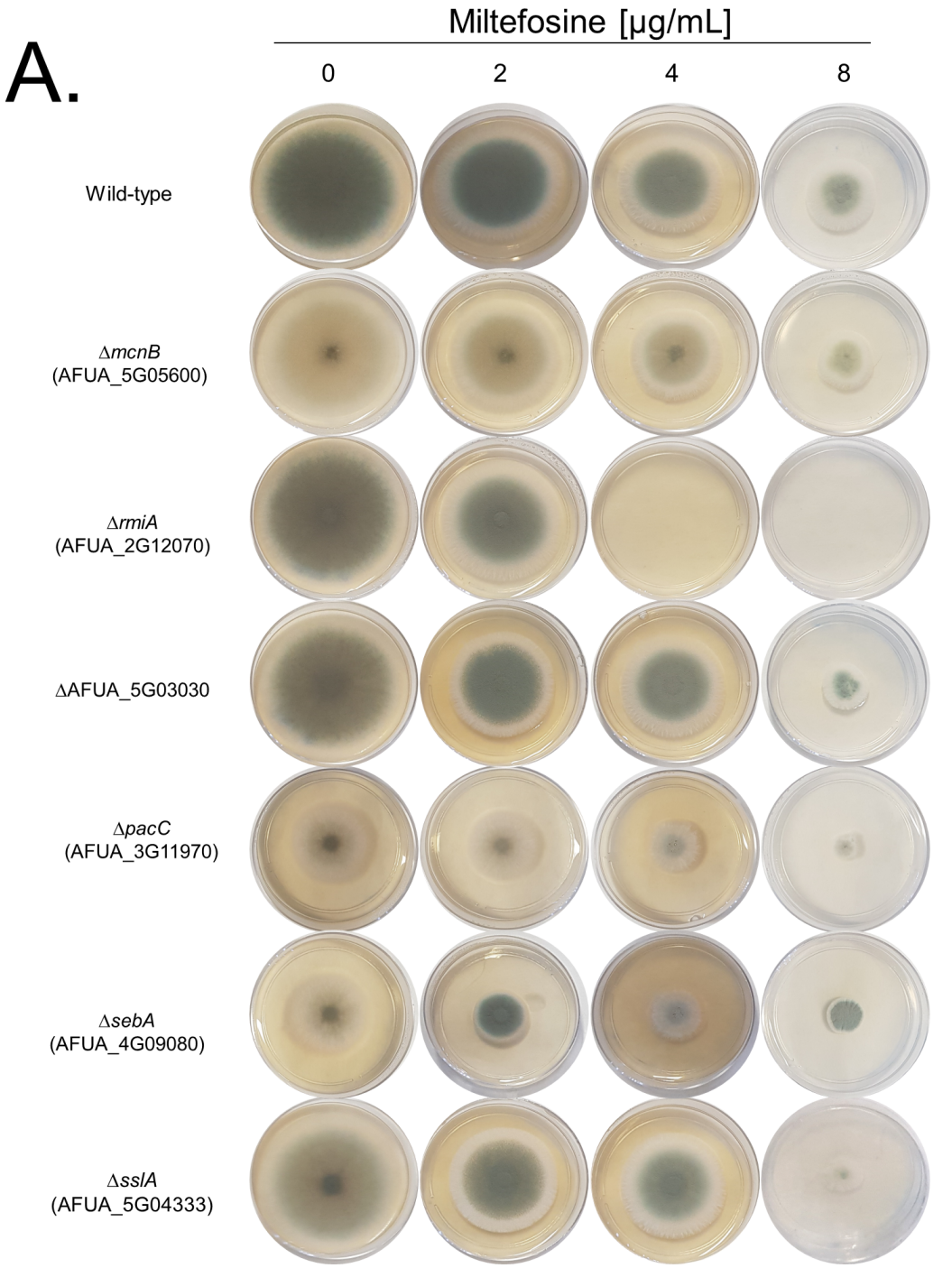
A.
Miltefosine [µg/mL]
0
2
4
8
Wild-type
ΔmcnB
(AFUA_5G05600)
ΔrmiA
(AFUA_2G12070)
ΔAFUA_5G03030
ΔpacC
(AFUA_3G11970)
ΔsebA
(AFUA_4G09080)
ΔsslA
(AFUA_5G04333)

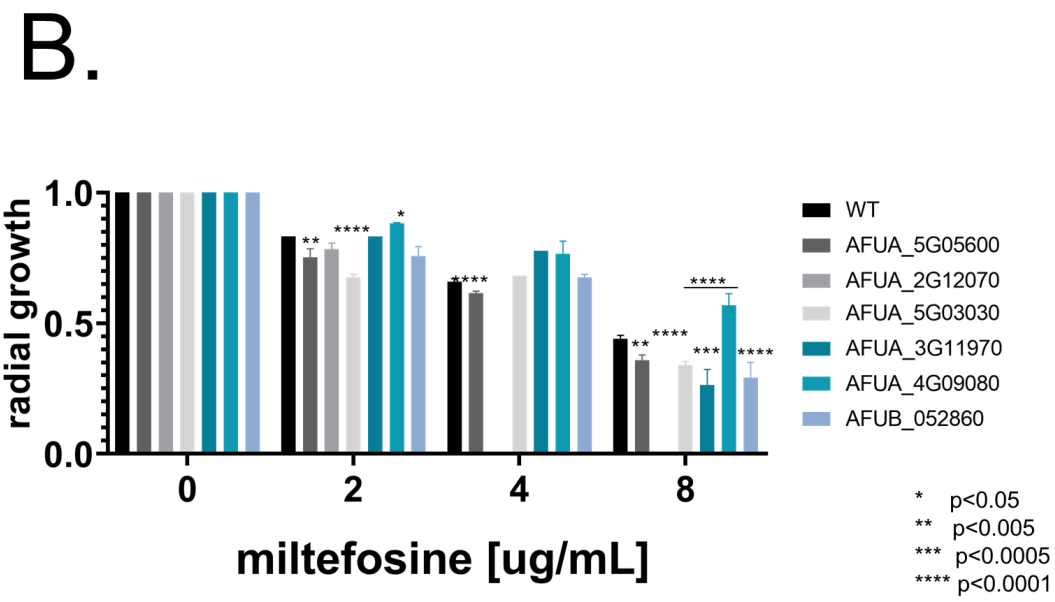
B.
radial growth
1.0
0.5
0.0
0
2
4
8
miltefosine [ug/mL]
WT
AFUA_5G05600
AFUA_2G12070
AFUA_5G03030
AFUA_3G11970
AFUA_4G09080
AFUB_052860
* p<0.05
** p<0.005
*** p<0.0005
**** p<0.0001

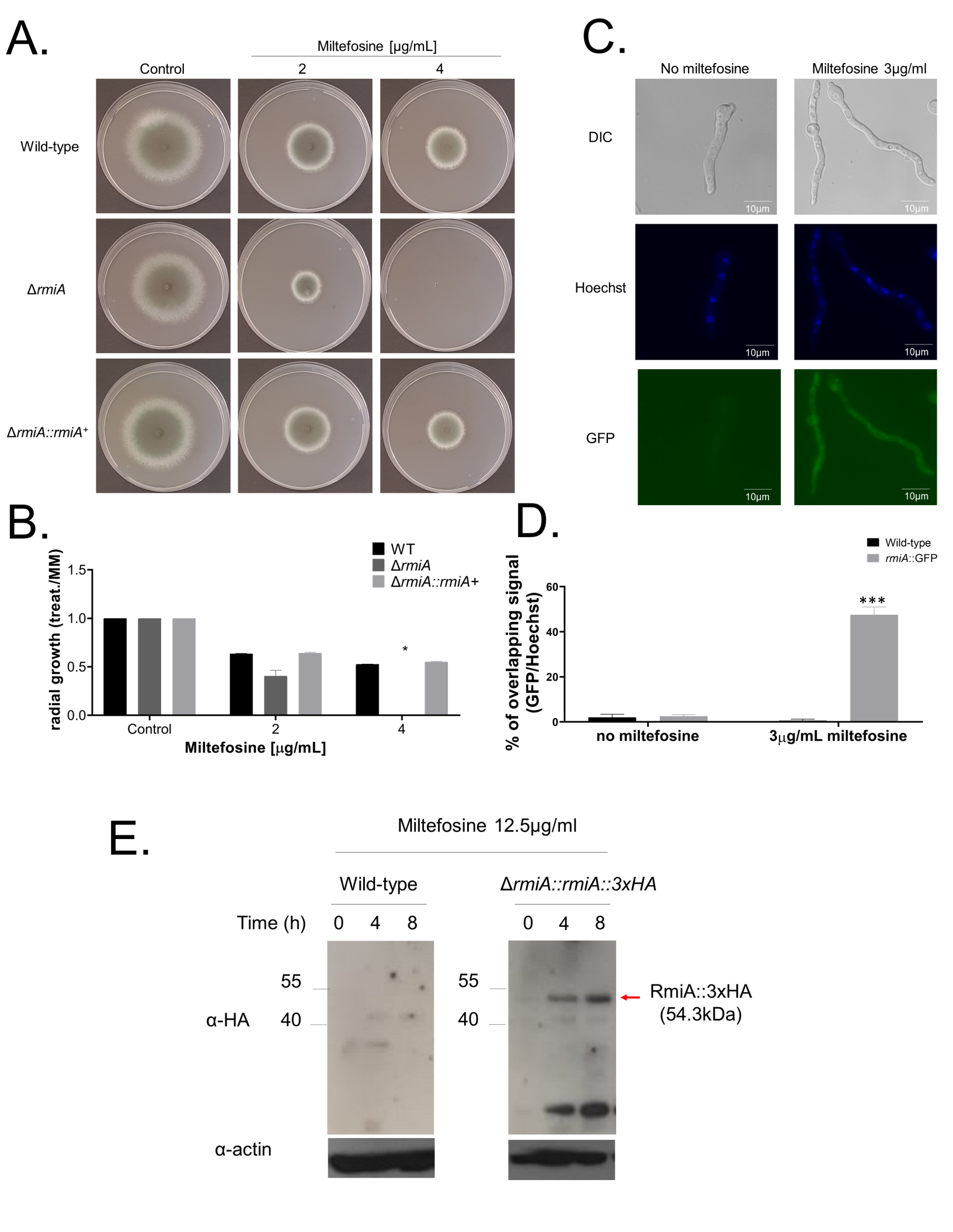
A.
Miltefosine [µg/mL]
Control
2
4
Wild-type
ΔrmiA
ΔrmiA::rmiA+
C.
No miltefosine
Miltefosine 3µg/ml
DIC
Hoechst
GFP
10µm
B.
WT
ΔrmiA
ΔrmiA::rmiA+
radial growth (treat./MM)
1.5
1.0
0.5
0.0
Control
2
4
*
Miltefosine [µg/mL]
D.
Wild-type
rmiA::GFP
% of overlapping signal (GFP/Hoechst)
60
40
20
0
***
no miltefosine
3µg/mL miltefosine
E.
Miltefosine 12.5µg/ml
Wild-type
ΔrmiA::rmiA::3xHA
Time (h)
0
4
8
55
40
α-HA
α-actin
RmiA::3xHA
(54.3kDa)

A.

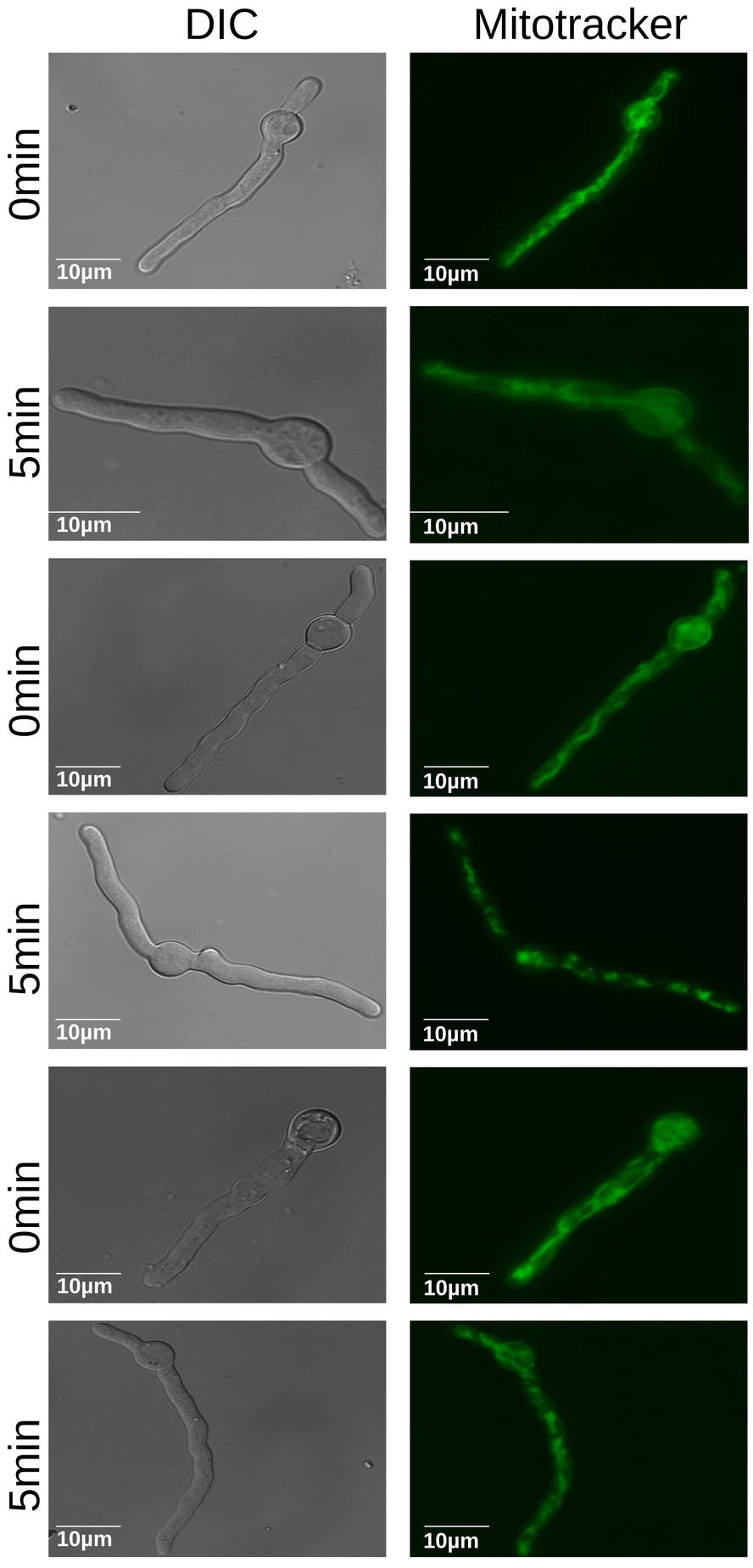

Wild-type

Δ*rmiA*

Δ*rmiA::rmiA*$^{+}$

B.

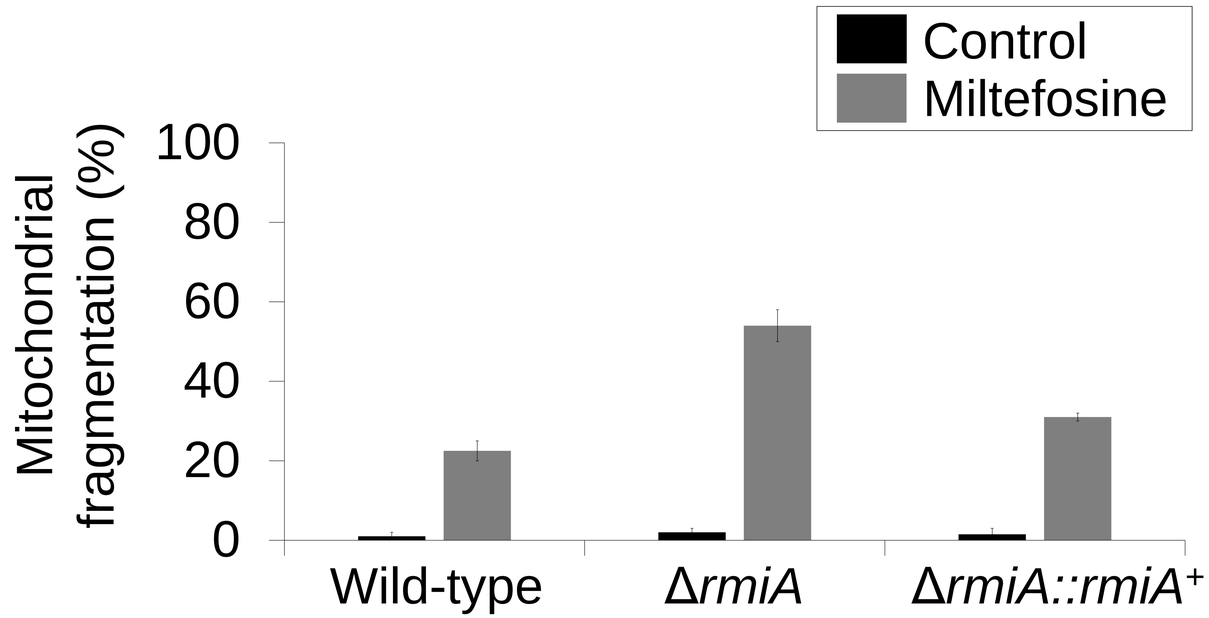

C.

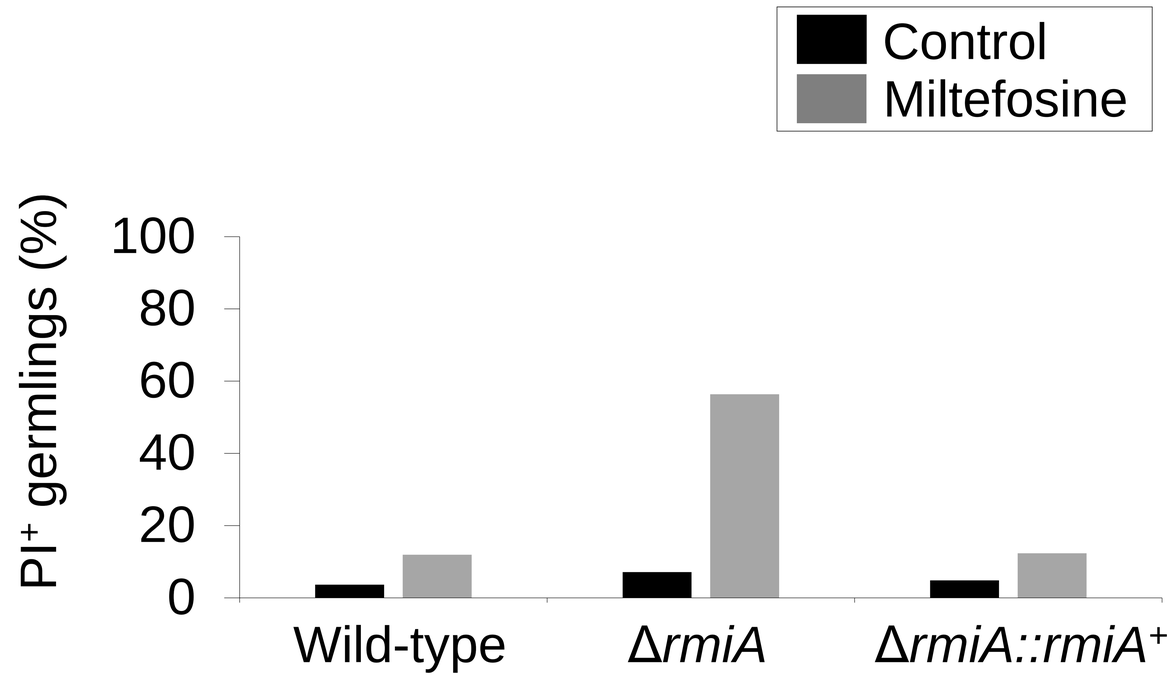

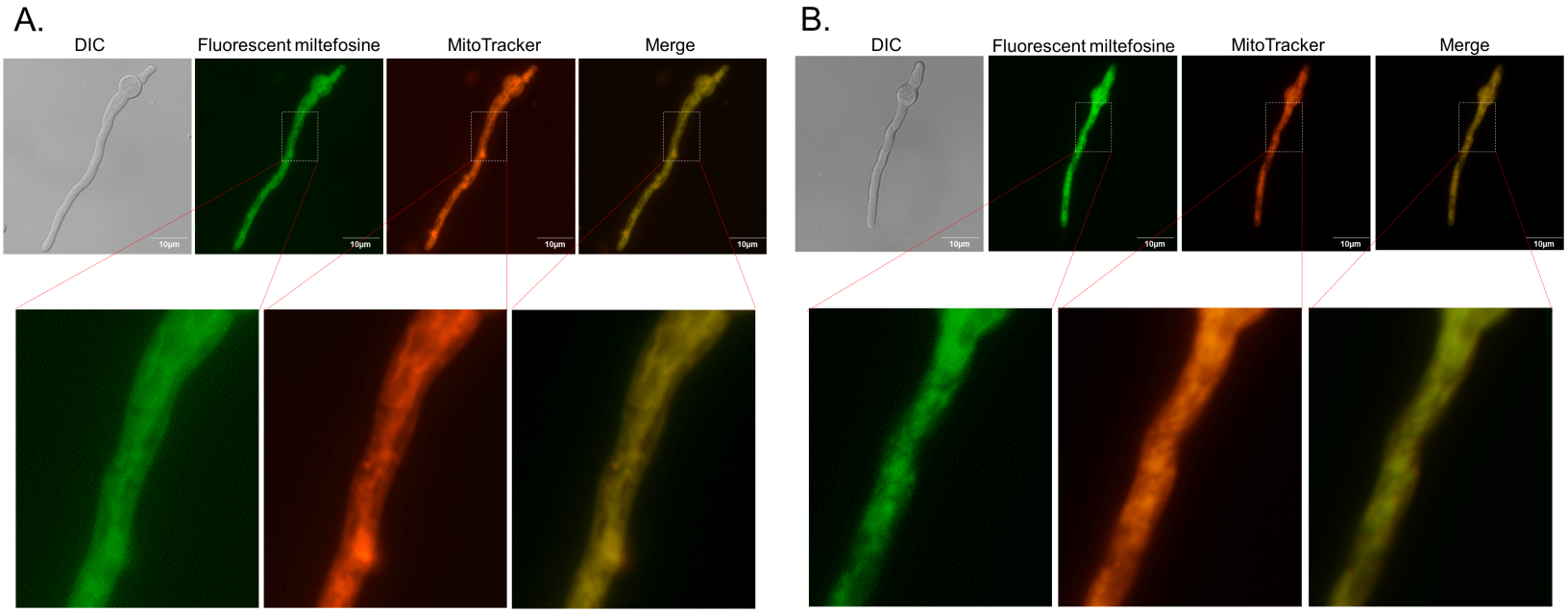
A.
DIC
Fluorescent miltefosine
MitoTracker
Merge
10µm
B.
DIC
Fluorescent miltefosine
MitoTracker
Merge
10µm

A. WT miltefosine x WT control

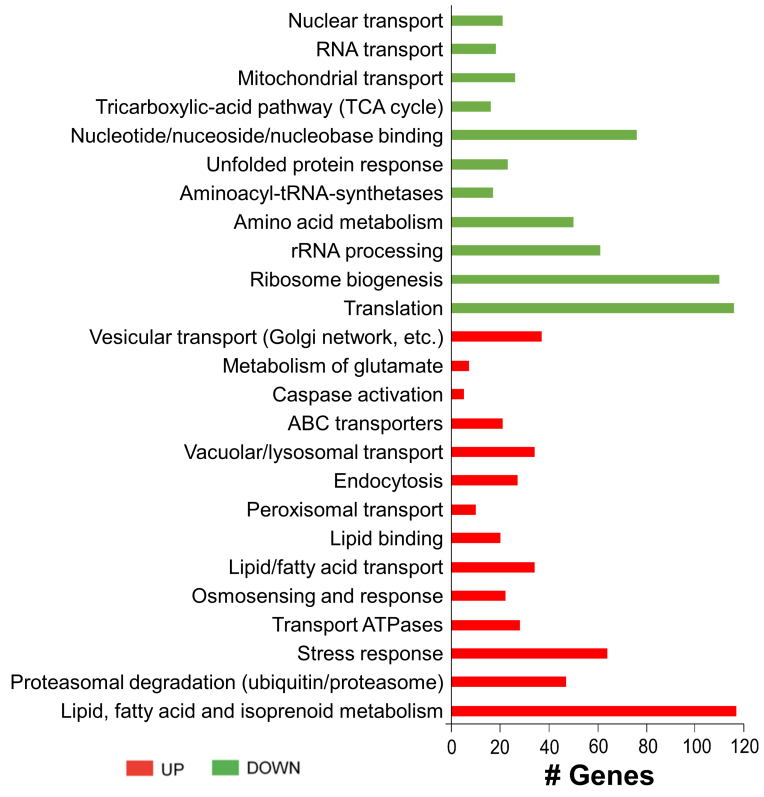

B. Δ*rmiA* miltefosine x Wild-type miltefosine

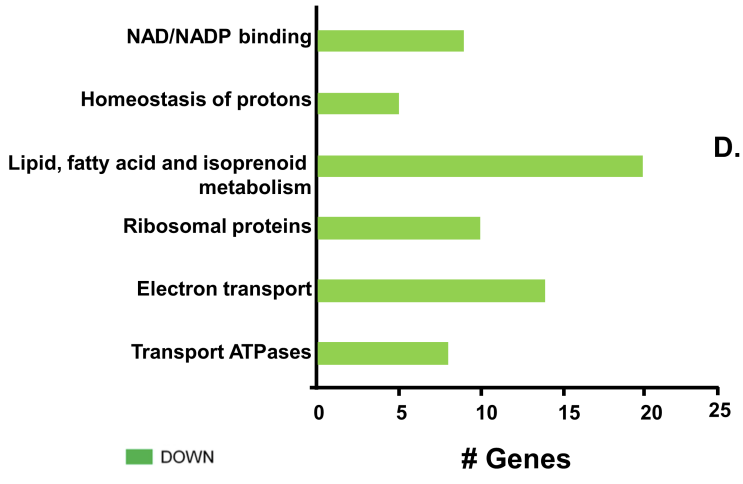

C.

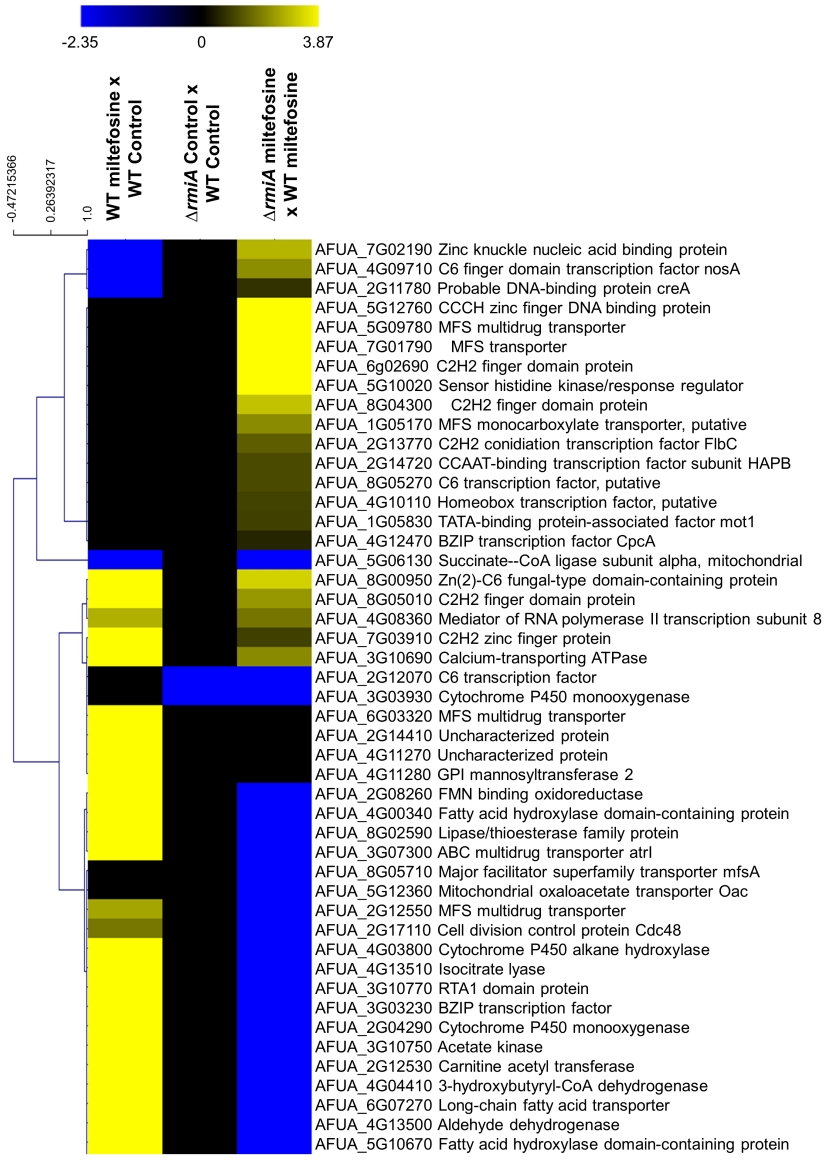

D.

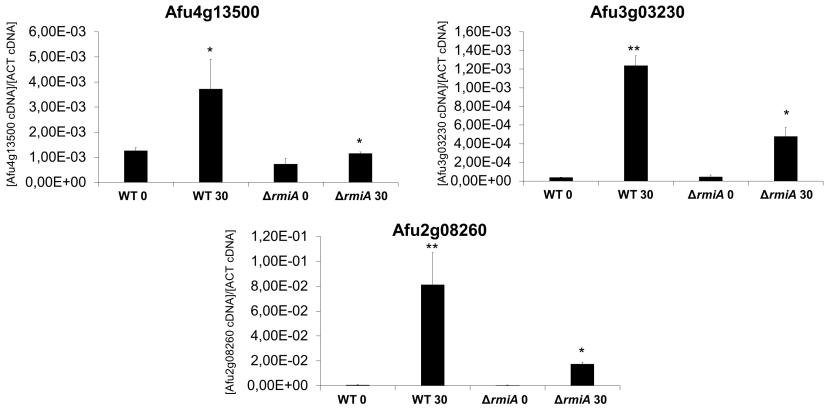

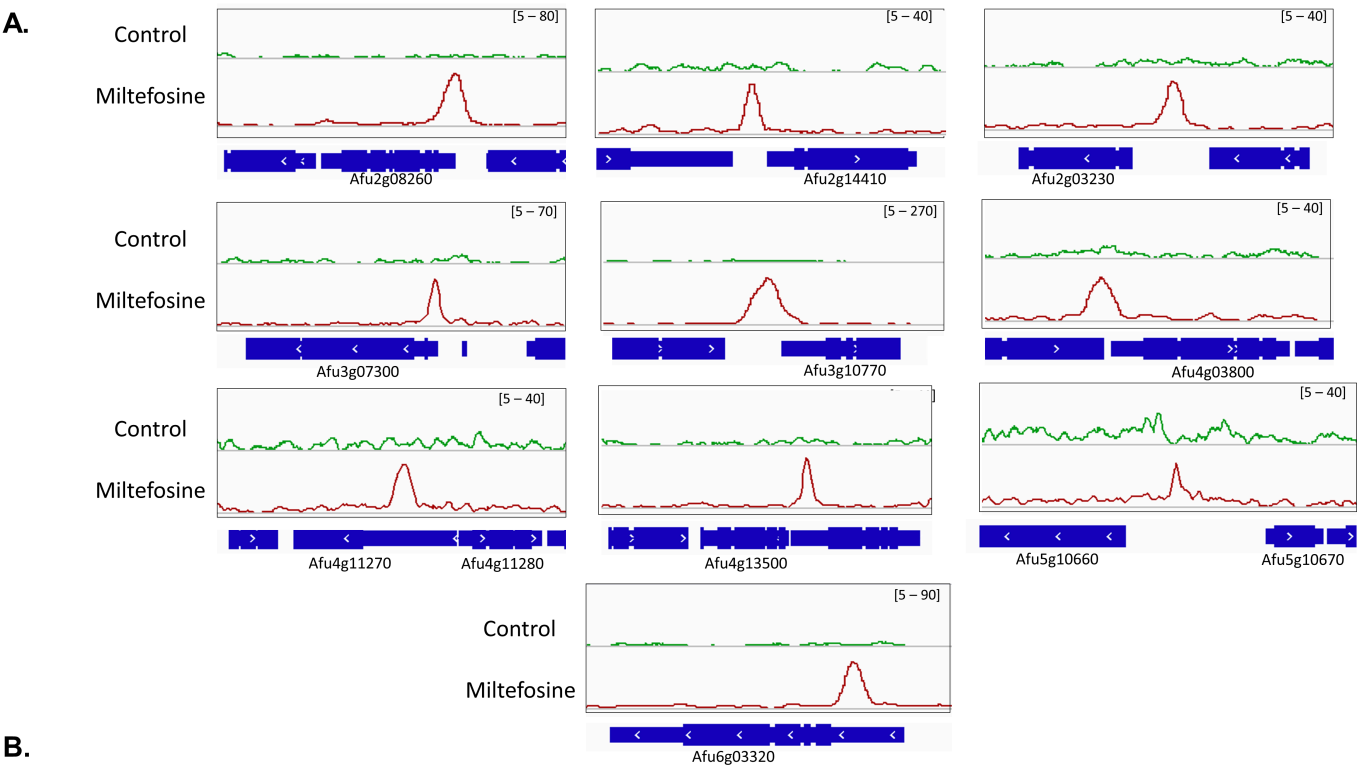

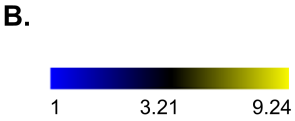

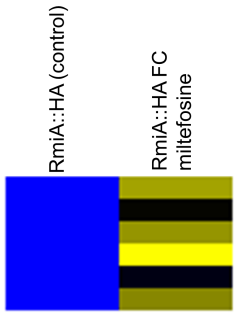

ChIP-seq

AFUA_2G08260 Oye2, FMN binding oxidoreductase
AFUA_3G03230 BZIP transcription factor
AFUA_3G07300 AtrA, ABC multidrug transporter
AFUA_3G10770 Rbs1, RTA 1 domain protein
AFUA_4g03800 Cytochrome P450 alkane hydroxylase
AFUA_4g13500 Hfd1, Aldehyde dehydrogenase

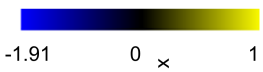

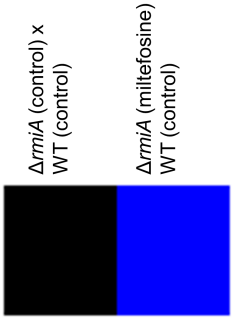

RNAseq

AFUA_2G08260 Oye2, FMN binding oxidoreductase
AFUA_3G03230 BZIP transcription factor
AFUA_3G07300 AtrA, ABC multidrug transporter
AFUA_3G10770 Rbs1, RTA 1 domain protein
AFUA_4g03800 Cytochrome P450 alkane hydroxylase
AFUA_4g13500 Hfd1, Aldehyde dehydrogenase

C.

Motif found
E-value: 0.038
Known or similar motifs:
SKO1 (MA0382.1)
TOD6 (MA0350.1)

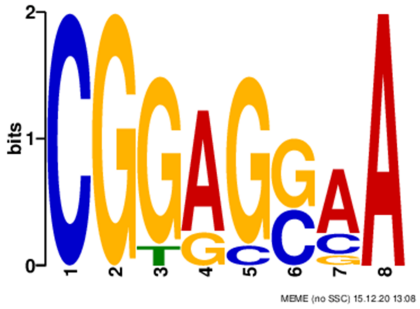

Motif found
E-value: 0.05
Known or similar motifs:
YPR196W (MA0437.1)
HAL9 (MA0311.1)

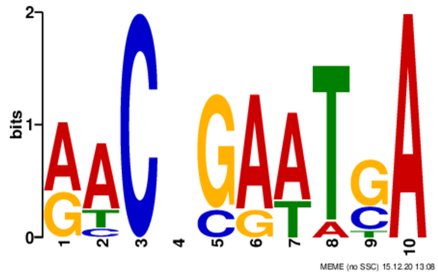

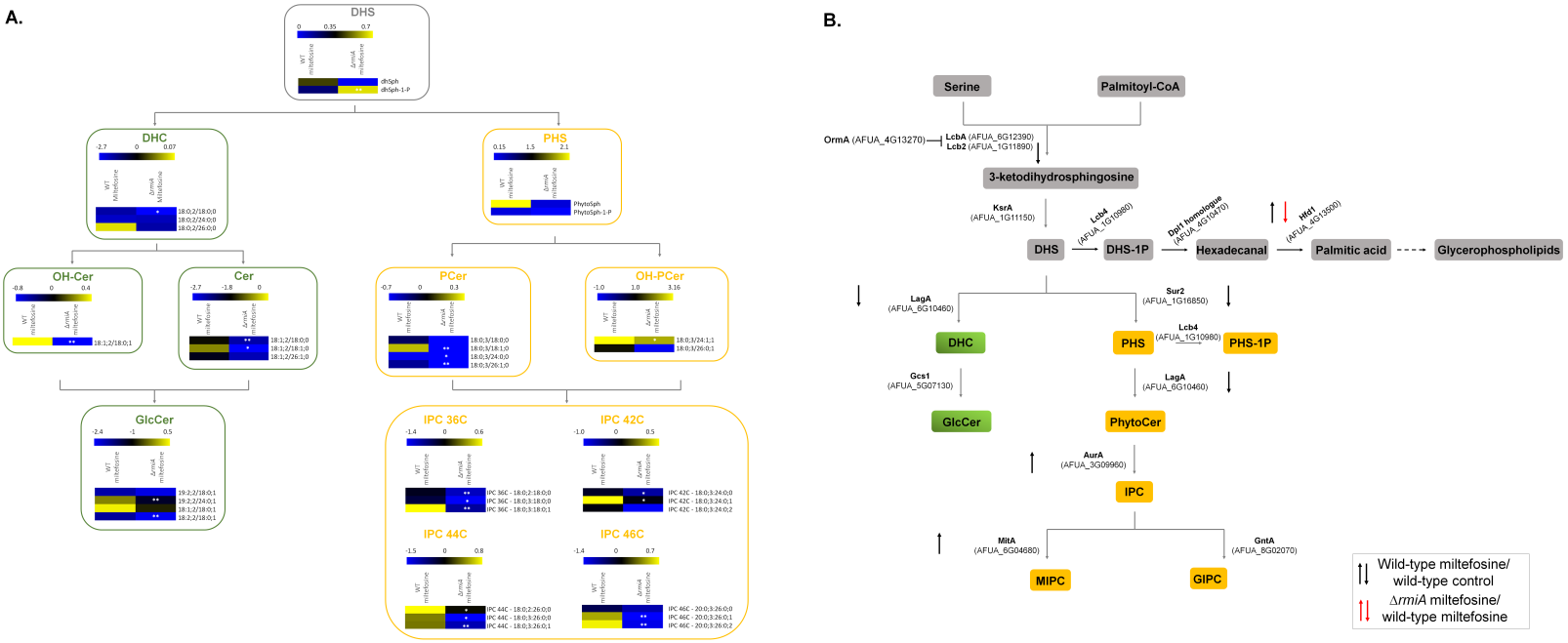
A.
DHS
0 0.35 0.7
WT miltefosine
ΔrmiA miltefosine
dhSph
dhSph-1-P
DHC
-2.7 0 0.07
18:0;2/18:0;0
18:0;2/24:0;0
18:0;2/26:0;0
PHS
0.15 1.5 2.1
PhytoSph
PhytoSph-1-P
OH-Cer
-0.8 0 0.4
18:1;2/18:0;1
Cer
-2.7 -1.8 0
18:1;2/18:0;0
18:1;2/18:1;0
18:1;2/26:1;0
PCer
-0.7 0 0.3
18:0;3/18:0;0
18:0;3/18:1;0
18:0;3/24:0;0
18:0;3/26:1;0
OH-PCer
-1.0 1.0 3.16
18:0;3/24:1;1
18:0;3/26:0;1
GlcCer
-2.4 -1 0.5
19:2;2/18:0;1
19:2;2/24:0;1
18:1;2/18:0;1
18:2;2/18:0;1
IPC 36C
-1.4 0 0.6
IPC 36C - 18:0;2:18:0;0
IPC 36C - 18:0;3:18:0;0
IPC 36C - 18:0;3:18:0;1
IPC 42C
-1.0 0 0.5
IPC 42C - 18:0;3:24:0;0
IPC 42C - 18:0;3:24:0;1
IPC 42C - 18:0;3:24:0;2
IPC 44C
-1.5 0 0.8
IPC 44C - 18:0;2:26:0;0
IPC 44C - 18:0;3:26:0;0
IPC 44C - 18:0;3:26:0;1
IPC 46C
-1.4 0 0.7
IPC 46C - 20:0;3:26:0;0
IPC 46C - 20:0;3:26:0;1
IPC 46C - 20:0;3:26:0;2
B.
Serine
Palmitoyl-CoA
OrmA (AFUA_4G13270)
LcbA (AFUA_6G12390)
Lcb2 (AFUA_1G11890)
3-ketodihydrosphingosine
KsrA (AFUA_1G11150)
Lcb4 (AFUA_1G10980)
Dpl1 homologue (AFUA_4G10470)
Hfd1 (AFUA_4G13590)
DHS
DHS-1P
Hexadecanal
Palmitic acid
Glycerophospholipids
LagA (AFUA_6G10460)
Sur2 (AFUA_1G16850)
DHC
PHS
Lcb4 (AFUA_1G10980)
PHS-1P
Gcs1 (AFUA_5G07130)
LagA (AFUA_6G10460)
GlcCer
PhytoCer
AurA (AFUA_3G09960)
IPC
MitA (AFUA_6G04680)
GntA (AFUA_8G02070)
MIPC
GIPC
Wild-type miltefosine/ wild-type control
ΔrmiA miltefosine/ wild-type miltefosine

A.

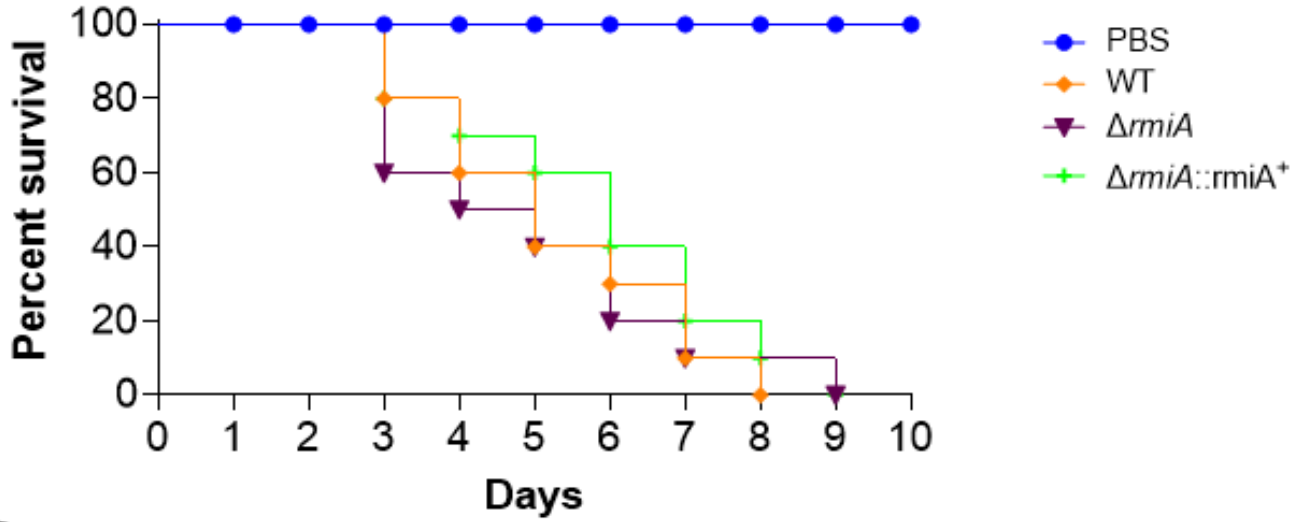
Percent survival
100
80
60
40
20
0
0 1 2 3 4 5 6 7 8 9 10
Days
PBS
WT
ΔrmiA
ΔrmiA::rmiA+

B.

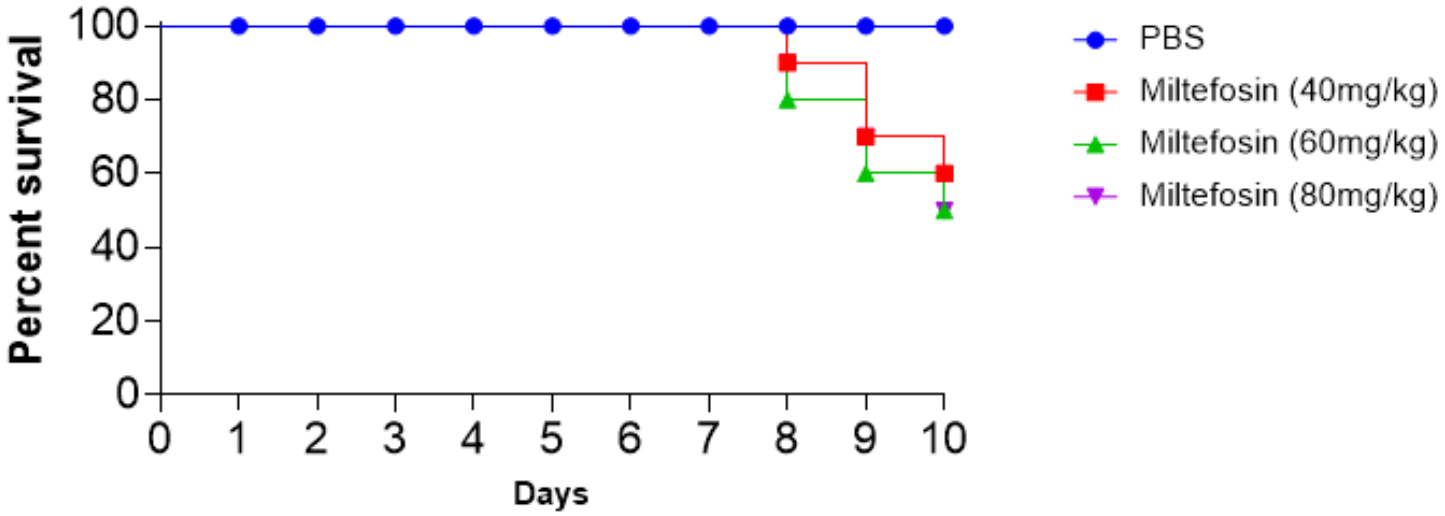
Percent survival
100
80
60
40
20
0
0 1 2 3 4 5 6 7 8 9 10
Days
PBS
Miltefosin (40mg/kg)
Miltefosin (60mg/kg)
Miltefosin (80mg/kg)

C.

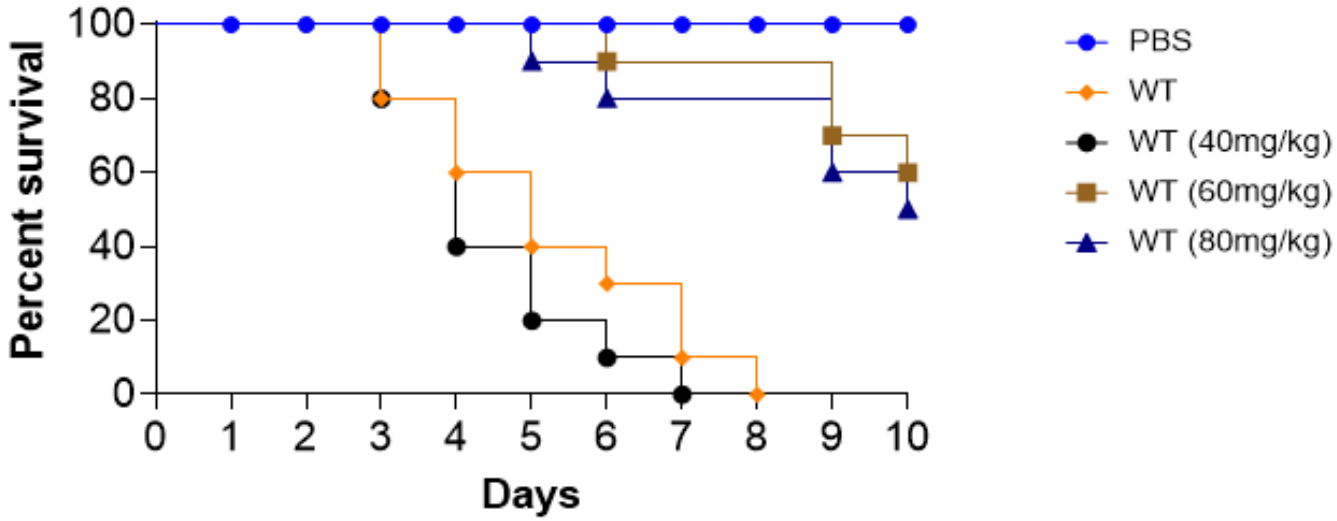
Percent survival
100
80
60
40
20
0
0 1 2 3 4 5 6 7 8 9 10
Days
PBS
WT
WT (40mg/kg)
WT (60mg/kg)
WT (80mg/kg)